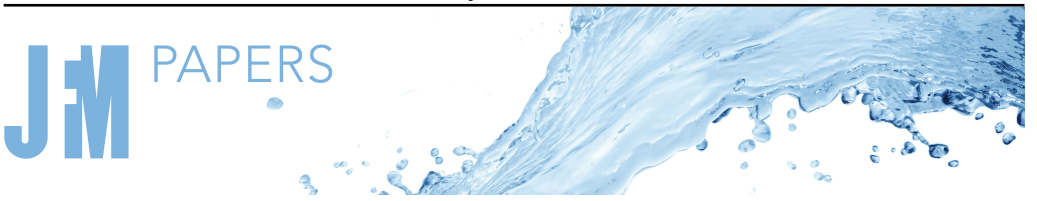
J. Fluid Mech. (2026), *vol.* 1044, A44, doi:10.1017/jfm.2026.12034



Vibrational non-equilibrium in high-speed combustion applications. 1. Modelling framework

Stephen Joseph Voelkel[1], **Mark Short**[1] **and Carlos Chiquete**[1]

[1]Los Alamos National Laboratory, Los Alamos, NM 87545, USA

Corresponding author: Stephen Joseph Voelkel, svoelkel@lanl.gov

(Received 27 July 2025 UTC; revised 1 April 2026 UTC; accepted 13 July 2026 UTC)

A new framework for modelling vibrational non-equilibrium in high-speed combustion is presented and evaluated. Our model builds upon a wide range of historical modelling paradigms to account for vibrational non-equilibrium exchange mechanisms, including translational–vibrational (T–V), vibrational–vibrational (V–V) and chemical–vibrational (C–V) processes, as well as vibrationally informed chemical reactions. Complementary forms of the T–V and V–V exchange processes are presented and compared, revealing how T–V exchange controls relaxation by driving each species towards vibrational equilibrium, whereas V–V exchange controls redistribution by driving each species towards a common, relative level of vibrational non-equilibrium. A modified form of the V–V exchange probability is proposed to ensure that vibrational energy does not leak into other modes. Additionally, a generalised vibrational efficiency function for complex reactions is derived. This form is subsequently used to derive the C–V exchange rate, which controls creation and destruction of vibrational energy from chemical reactions, resulting in a generalised, coupled vibration–chemistry–vibration model. Each of these processes (T–V, V–V and C–V exchange), as well as the vibrational efficiency function, is defined for general systems. We then examine each process in the context of high-speed combustion applications, in which temperatures are below 5000 K, and implement model simplifications where applicable. This model is used to predict the role of vibrational non-equilibrium in hydrogen chain-branching reactions and is shown to perform similarly to more complex, historical models. The model represents a physically grounded, tractable approach for including vibrational non-equilibrium effects in high-speed combustion applications.

Key words: detonation waves, hypersonic flow, gas dynamics

© The Author(s), 2026. Published by Cambridge University Press. This is an Open Access article, distributed under the terms of the Creative Commons Attribution-NonCommercial-NoDerivatives licence (https://creativecommons.org/licenses/by-nc/4.0/), which permits non-commercial re-use, distribution, and reproduction in any medium, provided that no alterations are made and the original article is properly cited. The written permission of Cambridge University Press or the rights holder(s) must be obtained prior to any commercial use and/or adaptation of the article.

https://doi.org/10.1017/jfm.2026.12034 Published online by Cambridge University Press

1. Introduction

The role of thermal non-equilibrium in hypersonics and high-speed combustion has been extensively studied since the 1950s. Non-equilibrium is prevalent after shock waves and rapid flow expansions in high-speed flows, where the internal (rotational and vibrational) motion of molecules takes time to respond to the rapid compression (or expansion) associated with the bulk flow (Boyd & Schwartzentruber 2017). The system relaxes back towards equilibrium over a corresponding relaxation time scale. This process is particularly relevant in atmospheric reentry dynamics (Gnoffo 1999), shock trains (Fiévet & Raman 2018), turbulent hypersonic boundary layers (Passiatore *et al.* 2022), supersonic combustion (Fiévet *et al.* 2017) and detonations (Voelkel *et al.* 2016*a*). More broadly, in any system where the relaxation time scale is comparable to chemical, hydrodynamic and bulk flow time scales associated with the system, non-equilibrium can play an important role in the flow physics by modifying reaction time scales, thermodynamic properties, heat release, stability and more. Vibrational non-equilibrium is of particular interest in air- and hydrogen-based applications due to the large relaxation time scales observed (Vincenti & Kruger 1965).

Detailed models for vibrational non-equilibrium physics have been developed for hypersonic flight and reentry flows (Hall *et al.* 1962; Lee 1965, 1985; Candler & MacCormack 1988, 1991; Park 1993; Gnoffo 1999; Panesi *et al.* 2013; Candler 2019; Passiatore *et al.* 2022; Du *et al.* 2023; Schramm *et al.* 2023; Chaudhry *et al.* 2025; Varma & Zhong 2025), which are often characterised by temperatures exceeding 5000 K. For such temperatures, non-equilibrium processes exhibit some unique relaxation processes, including enhanced rotational non-equilibrium (Panesi *et al.* 2013), strong coupling of vibrational relaxation among species (Candler & MacCormack 1988, 1991), ionisation (Lee 1985) and rarefied flow conditions (Boyd 1990*b*); consequently hypersonic reentry flow models are not typically applicable at the lower temperatures associated with high-speed combustion (Voelkel *et al.* 2016*a*). In contrast, due to the complex nature of the larger molecules and detailed reaction mechanisms, studies of hydrogen/hydrocarbon-based combustion in high-speed applications have often employed more limited modelling paradigms for vibrational non-equilibrium. However, due to the nature of combustion in such systems, where small perturbations can significantly affect ignition and flow stability, a physically complete and internally consistent model needs to be employed. Thus, this work seeks to establish a robust and defensible modelling framework for describing the fundamental underlying physics associated with vibrational non-equilibrium within high-speed combustion applications, specifically supersonic combustion and detonations.

The foundational theory of non-equilibrium relaxation began in earnest with the seminal work by Landau & Teller (1936) that introduced a vibrational relaxation model via an exchange mechanism with translational energy during molecular collisions. This was followed by Schwartz–Slawsky–Herzfeld theory that extended the Landau–Teller theory with a generalised form of the vibrational exchange probability based on first principles that was valid for polyatomic molecules (Schwartz *et al.* 1952). This theory demonstrated that the exchange probability could be increased in two ways: (i) by introduction of a species that lessens the reduced mass of the colliding pairs (a mass effect) or (ii) by introduction of a species with two or more vibrational degrees of freedom or close spacing between vibrational modes (a resonance effect). Both of these observations support the notion of 'effective colliders' – molecules that enhance relaxation of other species within a mixture.

https://doi.org/10.1017/jfm.2026.12034 Published online by Cambridge University Press

These distinct physical processes led to two key modelling paradigms: (i) vibrational exchange with translational energy, denoted T–V exchange; and (ii) vibrational exchange with vibrational energy, denoted V–V exchange. Millikan & White (1963) collated relaxation measurements from a wide range of colliding molecular pairs, excluding those with resonance, thus limiting the relaxation times to those dominated by T–V exchange. They developed a robust correlation for calculating the relaxation time scale up to 8000 K for a wide range of molecules. Taylor *et al.* (1967) measured V–V exchange rates for various two-component mixtures and observed a critical coupling effect. In mixtures wherein one species (A) has a much greater T–V exchange rate than the other (B), A will initially relax rapidly until it reaches some fractional level of vibrational non-equilibrium. Beyond this point, the V–V process becomes more prevalent, and both A and B relax at a similar rate, with A 'pulling' B towards equilibrium through V–V exchange. Similar findings by White (1968), Fisher & Kummler (1968), Kung & Center (1975) and Center & Newton (1978) corroborated this observation.

These results collectively show that, broadly, T–V exchange drives relaxation by pushing each molecule towards thermal equilibrium, while V–V exchange drives redistribution by pushing each molecule towards a shared non-equilibrium state. It is now common to model each of these processes separately, typically via the Landau–Teller relation for T–V exchange, and the form presented by Candler & MacCormack (1988, 1991) for V–V exchange, with distinct relaxation time scales for each exchange process. Further work was also done to address rotational non-equilibrium and, subsequently, vibrational–rotational exchange (Secrest 1973). The exchange probabilities for T–V and V–V exchange vary considerably depending on the application, and many correlations, corrections and best practices are discussed throughout this work.

In conjunction with these foundational works directed towards understanding vibrational relaxation via T–V and V–V exchange, significant modelling efforts were directed towards hypersonic flight and understanding the thermal and structural load experienced by a capsule during atmospheric reentry (Hall *et al.* 1962; Lee 1965). At such conditions, shock waves result in significant vibrational non-equilibrium (along with other effects, such as rotational non-equilibrium and ionisation) between the shock and the surface of the capsule (or aircraft). Dissociation rate measurements of O_2 and N_2 at these conditions showed measurable impacts due to vibrational non-equilibrium (Hammerling *et al.* 1959; Treanor & Marrone 1962; Wray & Teare 1962; Marrone & Treanor 1963). Because these rates directly control the heat release and subsequent heating of the capsule, accurate modelling of vibrationally informed chemical rates became a critical aspect of non-equilibrium theory.

Early modelling efforts directed towards coupling vibrational non-equilibrium and chemical dissociation were led by Hammerling *et al.* (1959) with the development of the CVD (coupled vibration–dissociation) model, which leveraged a vibrational efficiency function, defined as the ratio between the non-equilibrium and equilibrium rate. The CVD model assumed that dissociation occurs with equal probability from any vibrational state that has sufficient translational energy to cross the dissociation barrier, i.e. as vibrational energy increases, so too does the reaction rate. Shortly thereafter, Treanor & Marrone (1962) developed the CVDV (coupled vibration–dissociation–vibration) model, an extension of the CVD model that described how dissociation modified the vibrational state of the system, commonly referred to as chemical–vibrational (C–V) exchange. Later, Knab *et al.* (1995) developed the CVCV (coupled vibration–chemistry–vibration) model, a further extension of the CVDV model that accounts for exchange and associative ionisation reactions with finite reaction barriers. More recently, Arsentiev *et al.* (2012) incorporated the activation barrier associated with reverse reactions into the efficiency function.

https://doi.org/10.1017/jfm.2026.12034 Published online by Cambridge University Press

In conjunction with the CVCV-like models, which themselves have limits in their assumption of a Boltzmann distribution (especially for translational temperatures between 20 000 and 60 000 K), other modelling paradigms have been employed for reentry applications, perhaps none more impactful than Park's two-temperature model (Park 1988, 1989). Here, a representative vibrational temperature is transported along with the flow equations, and the reaction rate is modified based on an averaging of the translational and vibrational temperatures. The resulting correlation-based model proved to be computationally efficient while still accurately predicting key physical quantities of interest associated with the reentry problem (Candler & MacCormack 1991; Park 1993). In more recent years, the modified Marrone–Treanor model has also been developed for dissociating air at high temperatures (Chaudhry & Candler 2019; Chaudhry *et al.* 2025). Like Park's model, a single, representative vibrational temperature is used for the mixture, but coupled vibration–chemistry–vibration considerations are also employed, resulting in a robust model for high-temperature flows. The key assumption though, that all species relax towards a common relative vibrational state (and thus a common vibrational temperature), breaks down at lower temperatures where V–V exchange is less dominant (Reising *et al.* 2016).

Other approaches for overcoming the limiting assumptions of the CVCV-like models were to directly simulate the evolution of individual vibrational modes associated with each species (a state-to-state formulation) or to leverage direct simulation Monte Carlo in rarefied flow conditions (Boyd 1990*b*; Gallis *et al.* 2010; Panesi *et al.* 2013). Typically, these approaches require significantly greater computational resources. In particular, the state-to-state method necessitates additional transport equations for each vibrational mode of each species. Beyond this point, describing the vibrational exchange processes via both inter- and intramolecular collisions is highly non-trivial. Semi-classical modelling efforts such as the forced harmonic oscillator model (Adamovich *et al.* 1995; Macheret & Adamovich 2000) or state-specific rates calculated via quasi-classical trajectory (QCT) simulations (Esposito *et al.* 2006; Panesi *et al.* 2014) are typically employed. More recent efforts consider a hybrid binning approach (Munafò *et al.* 2015) and machine-learning paradigms (Zanardi *et al.* 2023) for overcoming the limits of detailed state-to-state modelling approaches. Even so, these methods remain limited to systems without complex polyatomic species and large chemical mechanisms, such as those in hydrogen/hydrocarbon combustion.

Beyond the reentry problem, the role of vibrational non-equilibrium has also been examined in less extreme environments, such as those within high-speed combustion applications. Much of the early modelling efforts within this regime were informed by the historical work associated with the reentry problem. Starik & Titova (2001) first demonstrated the role of vibrational non-equilibrium in hydrogen–air detonation profiles, using complex models for vibrational efficiency and T–V, V–V and C–V exchange. This model was later extended to examine CH_4 combustion (Lukhovitskii *et al.* 2008). Taylor *et al.* (2013*a*,*b*) showed that the T–V relaxation process associated with shocked stoichiometric H_2–air mixtures occurred on the same relative time scales as chemical reactions. Using a simplified two-temperature model, Koo *et al.* (2015) simulated supersonic combustion within a co-flow configuration and observed a significant delay in flame ignition and a reduced heat release. Fiévet *et al.* (2017) simulated combustion using a CVCV-like model with a vibrational efficiency function partially informed by QCT analysis, observing that cross-stream fuel injection played a critical role in flame ignition. Fiévet & Raman (2018), using a similar model to examine the effect of vibrational non-equilibrium in an isolator shock structure, observed a considerable change

https://doi.org/10.1017/jfm.2026.12034 Published online by Cambridge University Press

in the pseudo-shock structure to accommodate low vibrational temperatures associated with N_2.

These works collectively demonstrated that vibrational relaxation time scales are not negligible relative to the bulk flow and reaction time scales within high-speed combustion applications, and that non-equilibrium processes directly affect the flow field and combustion dynamics. Similar non-equilibrium models have also been applied to detonating flows. Voelkel *et al.* (2016*a*) showed that non-equilibrium only marginally affected the induction zone in Zel'dovich–von Neumann–Döring detonation waves of H_2–air mixtures. However, a much greater effect was observed in the two-dimensional detonations, with the presence of vibrational non-equilibrium increasing the detonation cell size by a factor of two. While this model included T–V and V–V exchange terms, as well as a QCT-informed efficiency function, only a rudimentary C–V exchange model was employed. Shi *et al.* (2017) corroborated these findings, and considered a range of models in their assessment. However, only a single vibrational temperature was utilised, V–V and C–V exchanges were neglected and the parameters associated with the Park and CVCV models were calibrated for reentry flows at much greater temperatures. Using an idealised detonation model with vibrational non-equilibrium (Park's two-temperature model with V–V and C–V exchange neglected), Uy *et al.* (2018) observed that the sensitivity of the induction zone to the activation energy was amplified by non-equilibrium. Beyond continuum-scale models, Yang *et al.* (2019) used direct simulation Monte Carlo to simulate one-dimensional H_2-O_2 detonations and observed reduced chain reaction rates due to under-excited vibrational states of the reactants. A meaningful C–V exchange effect was also observed, which significantly decreased the vibrational energy of reactants while increasing the vibrational energy of H_2O. Similar observations have been noted in recent state-to-state modelling efforts (Kadochnikov & Arsentiev 2020; Vargas *et al.* 2022). Importantly, only a subset of the species was treated using the state-to-state approach, with larger complex molecules, such as H_2O, relegated to simplified model descriptions.

Though early high-speed combustion studies relied heavily on the modelling choices associated with the reentry problem, it became clear that some of these choices were less accurate at lower temperatures (below 5000 K). Reising *et al.* (2016) measured rotational and vibrational temperatures of N_2 and O_2 within high-speed turbulent diffusion flames and demonstrated that the V–V exchange probability should be lowered compared with the values used for reentry applications. Voelkel *et al.* (2016*b*) utilised QCT theory to calculate the vibrational efficiency for key chain reactions in hydrogen combustion, and observed a significantly reduced role of vibrational non-equilibrium compared with Park's original model. More recently, experimental investigations by Chavez *et al.* (2023), Shi *et al.* (2024) and Zangene & Radulescu (2025) have suggested that vibrational non-equilibrium may contribute substantially less to detonation propagation than numerical studies have suggested, resulting in the postulation that vibrational non-equilibrium might have a negligible effect on chain reactions, or that other factors such as wall losses may play a more dominant role in detonation dynamics.

To address some of the modelling shortcomings in previous studies, this work presents a new, comprehensive formulation for modelling vibrational non-equilibrium, derived specifically for high-speed combustion applications. The formulation is largely motivated by historical, high-fidelity modelling efforts, with new functional relations, updated parameters and simplifying assumptions applied as relevant. The result is a tractable, physically consistent and robust model for examining arbitrary reactive systems in the high-speed combustion regime. We believe that the use of this model, with its inclusion of all critical non-equilibrium processes, in conjunction with its relatively simple form,

https://doi.org/10.1017/jfm.2026.12034 Published online by Cambridge University Press

will enable rigorous analysis of vibrational non-equilibrium processes in a wide range of high-speed applications.

In § 2, we present the continuum-scale governing equations for a vibrational non-equilibrium flow. A vibrationally partitioned, partial-pressure model is employed for the equation of state, and additional transport equations for the vibrational energy are defined. Section 3 describes the general form of the constitutive relations for vibrational non-equilibrium. The T–V exchange rates are based on the standard Landau–Teller form, and V–V exchange rates follow Candler & MacCormack (1988, 1991) and Knab *et al.* (1995), with an important modification to ensure that V–V exchange does not 'leak' into translational–rotational energy. Vibrationally informed chemical reactions are modelled via Arrhenius kinetics and modified via a vibrational efficiency function. The vibrational efficiency function itself is an extension and generalisation of the CVCV model derived for an arbitrary set of reactants and products with additional considerations for reverse reactions and a generalised efficiency function form. The C–V exchange rates are derived directly from chemical kinetics and thus still represent a coupled vibration–chemistry–vibration model. In § 4, we apply this modelling framework to a specific application – high-speed combustion flows with temperatures below 5000 K, including supersonic combustion and typical detonation conditions. Parameter ranges are evaluated and reduced forms are selected based on empirical observations within this regime. Finally, § 5 examines the role of vibrational non-equilibrium in chemical reactions, including comparisons with historical models for chain reactions in hydrogen combustion.

2. Governing equations

For a system exhibiting vibrational non-equilibrium, a single-temperature description of the internal energy does not exist, thus necessitating a vibrationally partitioned definition for the equation of state, as well as additional transport equations for the vibrational energy. Here, we describe this framework.

2.1. *Vibrationally partitioned equation of state*

Consider the ith species within some mixture, and assume it may be treated as an ideal gas. This species is considered to be in thermal equilibrium within some volume, V, if the probability distribution function (PDF) value of the $\boldsymbol{n}$th quantised molecular energy level, denoted $\widetilde{f}_i(\boldsymbol{n})$, is determined via a Boltzmann distribution with a single temperature (Vincenti & Kruger 1965), i.e.

$$\widetilde{f}_i(\boldsymbol{n}) = \frac{\mathrm{e}^{-\widetilde{\varepsilon}_i(\boldsymbol{n})/T_i}}{Q_i(T)}, \quad Q_i(T) = \sum_{\boldsymbol{n}} \mathrm{e}^{-\widetilde{\varepsilon}_i(\boldsymbol{n})/T_i}, \tag{2.1}$$

where $Q_i(T)$ is the species partition function of molecular energy states, $\widetilde{\varepsilon}_i(\boldsymbol{n})$ is the species' $\boldsymbol{n}$th energy state expressed in units of temperature and T_i is the species temperature. The $\widetilde{\cdot}$ notation is used to denote state-specific quantities that depend on the quantum state.

If the system is not in thermal equilibrium, then the definition of $\widetilde{f}_i(\boldsymbol{n})$ in (2.1) must be reconsidered. Following convention (Vincenti & Kruger 1965; McQuarrie 2000), we assume that $\widetilde{\varepsilon}_i(\boldsymbol{n})$ can be partitioned into translational (t), rotational (r), vibrational (v) and electronic (el) energy components so that

$$\widetilde{\varepsilon}_i(\boldsymbol{n}) = \widetilde{\varepsilon}_{t,i}(n_t) + \widetilde{\varepsilon}_{r,i}(n_r) + \widetilde{\varepsilon}_{v,i}(n_v) + \widetilde{\varepsilon}_{el,i}(n_{el}), \tag{2.2}$$

https://doi.org/10.1017/jfm.2026.12034 Published online by Cambridge University Press

where the subscript denotes the component, and the energy state $\boldsymbol{n}$ is now represented as a vector of quantum numbers for the translational, rotational, vibrational and electronic state, i.e. $\boldsymbol{n} = (n_t, n_r, n_v, n_{el})$. We assume that coupled rotational–vibrational energy can either be neglected (via the rigid-rotor approximation) or be subsumed into either the vibrational or rotational energy component. Substituting (2.2) into (2.1), and assuming each component is characterised by a component temperature, $T_{\alpha,i}$, the PDF becomes

$$\widetilde{f}_i(\boldsymbol{n}) = \prod_{\alpha} \left(\frac{\mathrm{e}^{-\widetilde{\varepsilon}_{\alpha,i}(n_\alpha)/T_{\alpha,i}}}{Q_{\alpha,i}(T_{\alpha,i})} \right), \quad Q_{\alpha,i}(T_{\alpha,i}) = \sum_{n_\alpha} \mathrm{e}^{-\widetilde{\varepsilon}_{\alpha,i}(n_\alpha)/T_{\alpha,i}}, \tag{2.3}$$

for $\alpha = t,\ r,\ v$ and el. When $T_{\alpha,i} = T_i$ for all α, the species is in thermal equilibrium and (2.1) is attained. Otherwise, the system is in a state of non-equilibrium.

With a PDF that accounts for thermal non-equilibrium, we are able to determine non-equilibrium relations for the internal energy and pressure. From the component partition functions in (2.3) and Boltzmann's entropy relation (Vincenti & Kruger 1965), the state-averaged (continuum-scale) specific internal energy and pressure components are given by

$$e_{\alpha,i} = \frac{\mathcal{R}_u T_{\alpha,i}^2}{W_i} \cdot \frac{\partial \left(\ln Q_{\alpha,i}\right)}{\partial T_{\alpha,i}}, \quad p_{\alpha,i} = \frac{M_i \mathcal{R}_u T_{\alpha,i}}{W_i} \cdot \frac{\partial \left(\ln Q_{\alpha,i}\right)}{\partial V}, \tag{2.4}$$

where $\mathcal{R}_u$ is the universal gas constant, W_i is the species molar mass and M_i is the total mass of the species within the volume, V. The details associated with the component forms of energy and pressure are described in Vincenti & Kruger (1965). Here, we include a brief summary of assumptions and associated results. For the translational and rotational energy, we assume the spacing between $\widetilde{\varepsilon}_{t,i}$ and $\widetilde{\varepsilon}_{r,i}$ states is small at the temperatures expected in high-speed combustion (above 300 K). It follows that $Q_{t,i}$ and $Q_{r,i}$ may be approximated by integrals rather than summations. For the vibrational energy, we will assume that some temperature-dependent oscillator model can be employed (e.g. the harmonic oscillator assumption). Finally, we note that the rotational, vibrational and electronic partition functions are independent of V, so $\partial(\ln Q_{\alpha,i})/\partial V = 0$ and $p_{\alpha,i} = 0$ for $\alpha = r,\ v,$ and el. In other words, the pressure only depends on the translational component of the internal energy.

Under these assumptions, the specific internal energy and pressure are defined as the summations of their respective components as defined in (2.4) and reduce to

$$e_i = e_{t,i}(T_{t,i}) + e_{r,i}(T_{r,i}) + e_{v,i}(T_{v,i}) + e_{el,i}(T_{el,i}), \quad p_i = \rho_i R_i T_{t,i}, \tag{2.5}$$

where $e_{t,i}$, $e_{r,i}$, $e_{v,i}$ and $e_{el,i}$ are the translational, rotational, vibrational and electronic components of the specific internal energy, respectively, each of which is characterised by a corresponding species- and mode-specific temperature. We assume $e_{el,i}$ includes the reference energy state associated with the enthalpy of formation. Additionally, ρ_i is the mass density, and $R_i = \mathcal{R}_u / W_i$ is the species-specific gas constant. At this stage, we do not prescribe a specific model for $e_{\alpha,i}$, except to note that each component is related to its corresponding temperature via a functional relationship. For a mixture of N species, the equation of state for ideal gas mixtures is typically based on Dalton's law of partial pressures (Powers & Paolucci 2005), with the mixture's internal energy and pressure given by

$$e = \sum_{i=1}^{N} Y_i e_i, \quad p = \sum_{i=1}^{N} p_i, \tag{2.6}$$

where Y_i is the species mass fraction.

https://doi.org/10.1017/jfm.2026.12034 Published online by Cambridge University Press

This mode-partitioned equation of state requires additional transport equations to evolve each mode independently, one for each independent mode. Additionally, we must account for the exchange of energy between modes and species, and determine how each energy component affects and responds to chemical reactions. For a broad range of systems in high-speed combustion, we can reduce the complexity considerably by applying a series of well-established assumptions. First, we assume that the translational energy of each molecular species relaxes within a few intermolecular collisions (Vincenti & Kruger 1965). It follows that the translational PDF for all molecular species will relax to a common translational temperature. Additionally, we also assume that rotational and electronic relaxation is rapid compared with the vibrational relaxation and chemical reaction processes in the high-speed combustion regime (Vincenti & Kruger 1965; Reising *et al.* 2016; Boyd & Schwartzentruber 2017). Even hydrogen, which has a relatively large characteristic rotational temperature of $\approx 90\,\mathrm{K}$ (Atkins *et al.* 2023), relaxes 2−4 times faster than vibrational modes at temperatures below 5000 K (Furudate *et al.* 2006). Thus, we assume that translational, rotational and electronic PDFs for all species can all be characterised by a single temperature associated with energy components that do not experience non-equilibrium, denoted the translational–rotational temperature, or T_{tr}.

These assumptions applied to (2.6) give

$$e = e_{tr}(T_{tr}) + \sum_{i=1}^{N} Y_i e_{v,i}, \qquad p = \rho R T_{tr}, \tag{2.7}$$

where $e_{tr} = \sum_i Y_i[e_{t,i}(T_{tr}) + e_{r,i}(T_{tr}) + e_{el,i}(T_{tr})]$ represents the mixture translational–rotational(–electronic) energy associated with T_{tr}; $\rho = \sum_i \rho_i$ is the mass density; and $R = \mathcal{R}_u / W$ is the specific gas constant, with $1/W = \sum_i Y_i / W_i$ denoting the average molar mass. Since the vibrational energy modes are decoupled from the internal energy associated with T_{tr}, additional equations must be employed to model the transport of the species' vibrational energy.

2.2. *Vibrationally partitioned transport equations*

The following transport equations are derived for a one-dimensional inviscid flow. Extending this derivation to viscous and higher-dimensional systems does not materially alter this underlying formulation. For a mixture with N species, the one-dimensional reactive Euler equations are given by

$$\frac{\partial}{\partial t}\begin{bmatrix} \rho \\ \rho u \\ \rho E \\ \rho Y_i \end{bmatrix} + \frac{\partial}{\partial x}\begin{bmatrix} \rho u \\ \rho u^2 + p \\ u(\rho E + p) \\ \rho u Y_i \end{bmatrix} = \begin{bmatrix} 0 \\ 0 \\ 0 \\ W_i \dot{\omega}_i \end{bmatrix}, \tag{2.8}$$

for $i = 1, \ldots, N$. Here, x and t denote the spatial and temporal components of the solution vector, respectively; u is the velocity; $E = e + u^2/2$ is the total energy; and $\dot{\omega}_i$ is the species molar production rate, with other variables defined in § 2.1.

Substituting the mixture internal energy (2.7) into the total energy transport equation (2.8) and rearranging gives

$$\sum_{i=1}^{N}\left[\frac{\partial}{\partial t}\left(\rho Y_i e_{v,i}\right) + \frac{\partial}{\partial x}\left(\rho u Y_i e_{v,i}\right)\right] + \left[\frac{\partial}{\partial t}\left(\rho E_{tr}\right) + \frac{\partial}{\partial x}\left(u(\rho E_{tr} + p)\right)\right] = 0, \tag{2.9}$$

https://doi.org/10.1017/jfm.2026.12034 Published online by Cambridge University Press

where $E_{tr} = e_{tr} + u^2/2$. Now, (2.9) may be posed as $N + 1$ separate transport equations for the vibrational energy and total translational–rotational–electronic energy given by

$$\frac{\partial}{\partial t}\left(\rho Y_i e_{v,i}\right) + \frac{\partial}{\partial x}\left(\rho u Y_i e_{v,i}\right) = S_i, \quad i = 1, \ldots, N, \tag{2.10a}$$

$$\frac{\partial}{\partial t}\left(\rho E_{tr}\right) + \frac{\partial}{\partial x}\left(u(\rho E_{tr} + p)\right) = -\sum_{i=1}^{N} S_i, \tag{2.10b}$$

where S_i is the species' vibrational energy exchange term, which governs the coupling of vibrational energy with other modes and its creation or destruction through chemical reactions. We choose a form given by

$$S_i = S_{T-V,i} + S_{V-V,i} + S_{C-V,i}, \tag{2.11}$$

where $S_{T-V,i}$ represents vibrational energy exchange of each species with translational–rotational–electronic energy of the mixture (denoted T–V exchange), $S_{V-V,i}$ represents vibrational energy exchange of each species with vibrational energy of all the other species in the mixture (denoted V–V exchange) and $S_{C-V,i}$ represents vibrational energy exchange via chemical reactions (denoted C–V exchange). As described in § 1, T–V exchange controls the relaxation process from vibrational non-equilibrium to equilibrium, V–V exchange controls the redistribution of vibrational energy among each species and C–V exchange controls the creation/destruction of vibrational energy from chemical reactions. Here, we do not include V–V–T exchange, which would account for non-equal spacing of quantised vibrational energy states between molecules in vibrational exchange collisions, by assuming that the corresponding contribution to the translational–rotational energy is negligible compared with T–V exchange (see § 3.2).

The set of equations in (2.10*a*) models the vibrational energy transport of each species. This, combined with the reactive Euler equations (2.8), completes the system of vibrationally partitioned transport equations. The translational–rotational energy transport equation (2.10*b*) is degenerate in this formulation, i.e. the translational–rotational energy can be calculated directly from the total and vibrational energies. As a final note, we recognise that the internal energy definition may be relaxed to include other non-equilibrium components, such as free-electron motion or rotational non-equilibrium. As such, additional transport equations are needed to close the system. A framework for extending the model to account for these considerations is discussed in Appendix A.

3. Constitutive relations for vibrational energy

We now look to define the constitutive relations for describing how vibrational energy couples with the other energy modes and processes in the system, beginning with translational–rotational energy (relaxation) and vibrational energy (redistribution). Then, we model how vibrational non-equilibrium informs chemical reactions, which may enhance or suppress the rate depending on the magnitude of vibrational energy relative to the translational–rotational state. Finally, we determine how energy creation/destruction via chemical reactions affects the vibrational energy.

3.1. *Translational–vibrational energy exchange*

Translational–vibrational energy exchange describes the coupling between translational and vibrational energy within the flow. In general, T–V exchange drives each species towards thermal equilibrium. For a harmonic oscillator, the exchange rate is of the

https://doi.org/10.1017/jfm.2026.12034 Published online by Cambridge University Press

Landau–Teller form (Landau & Teller 1936) given by

$$S_{T-V,i} = \sum_{j}^{N} S_{T-V,ij}, \quad S_{T-V,ij} = \frac{\rho Y_i e^{tr}_{v,i}}{\tau_{T-V,ij}/X_j} \cdot \left(1 - \frac{e_{v,i}}{e^{tr}_{v,i}}\right), \tag{3.1}$$

where $e^{tr}_{v,i}$ is the vibrational energy as defined in (2.5) evaluated at T_{tr}, $X_j = Y_i \cdot W/W_i$ is the species mole fraction and $\tau_{T-V,ij}$ is the species pairwise T–V relaxation time scale. The mixture-averaged time scale is given by $1/\tau_{T-V,i} = \sum_j X_j/\tau_{T-V,ij}$. In general, $\tau_{T-V,ij}$ depends on the molecular properties of the colliding pair, the translational–rotational temperature and the pressure, each of which in turn dictates the collision rate and probability of T–V exchange, i.e.

$$\tau_{T-V,ij} = \frac{\tau_{c,ij}}{P_{T-V,ij}}, \quad \tau_{c,ij} = \frac{W}{\rho\sigma_{ij}\mathcal{N}_A}\left(\frac{\pi W_{ij}}{8\mathcal{R}_u T_{tr}}\right)^{1/2}, \tag{3.2}$$

where $\tau_{c,ij}$ denotes the collision time scale, $P_{T-V,ij}$ is the exchange probability, σ_{ij} is the collision cross-section, $\mathcal{N}_A$ is Avogadro's number and $W_{ij} = W_i W_j/(W_i + W_j)$ is the reduced molar mass. Though this model was originally derived for harmonic oscillators, we assume that the relaxation time scale can be modified for more complex vibrational energy models by modifying $P_{T-V,ij}$ rather than altering the form of (3.1).

3.2. *Vibrational–vibrational energy exchange*

Vibrational–vibrational energy exchange models the coupling of vibrational energy among species within a mixture. In general, V–V exchange pushes each species to share the same relative vibrational state (Candler & MacCormack 1988, 1991). As such, $S_{V-V,i}$ may be either positive or negative, depending on the degree of vibrational non-equilibrium of each species in the mixture. The V–V exchange term is derived from the collision rate and the probability of exchange (Candler & MacCormack 1988, 1991), given by

$$S_{V-V,i} = \sum_{j\neq i}^{N} S_{V-V,ij}, \quad S_{V-V,ij} = W_i Z_{ij}\left(P_{V-V,ji} e_{v,j} - P_{V-V,ij} e_{v,i}\right), \tag{3.3}$$

where Z_{ij} is the (symmetric) collision rate and $P_{V-V,ij}$ and $P_{V-V,ji}$ are the (not necessarily symmetric) probability of species i increasing the local vibrational energy of species j and vice versa. In this form, $\sum_i S_{V-V,i}/W_i = 0$, so V–V exchange does not contribute to the production/destruction of molar-specific translational–rotational energy. At thermal equilibrium, we expect $S_{V-V,ij} = 0$, so, following Knab *et al.* (1992), $P_{V-V,ij}$ and $P_{V-V,ji}$ are constrained such that

$$P_{V-V,ji} e^{tr}_{v,j} = P_{V-V,ij} e^{tr}_{v,i}. \tag{3.4}$$

With this constraint, and with the collision rate as defined by Candler & MacCormack (1988, 1991), (3.3) reduces to the following form:

$$S_{V-V,ij} = \frac{\rho Y_i e^{tr}_{v,i}}{\tau_{V-V,ij}/X_j} \cdot \left(\frac{e_{v,j}}{e^{tr}_{v,j}} - \frac{e_{v,i}}{e^{tr}_{v,i}}\right), \quad \tau_{V-V,ij} = \frac{\tau_{c,ij}}{P_{V-V,ij}}, \tag{3.5}$$

where $\tau_{V-V,ij}$ is the species pairwise V–V redistribution time scale and $\tau_{c,ij}$ is the collision time scale as defined in (3.2). Similar to T–V exchange, the V–V exchange process pushes each species' vibrational energy to a specific value at a time scale based on the molecular collision rate and the associated exchange probability.

https://doi.org/10.1017/jfm.2026.12034 Published online by Cambridge University Press

It is important to note that this model assumes that the energy difference between any two vibrational state transitions is negligible. In other words, we do not account for non-equal spacing of quantised vibrational energy states between molecules. If we did, then V–V exchange collisions would either generate or require a small amount of excess translational–rotational energy as part of the exchange process, denoted V–V–T exchange. Here, we assume that this effect is negligible. Otherwise, we would need to employ a more extensive state-specific implementation that we compute and then average (at every unique temperature combination) to determine the state-averaged rate, significantly increasing the modelling/computational burden. To our knowledge, a reduced, state-averaged model that accounts for V–V–T exchange has not yet been developed, so to maintain a tractable modelling framework, and motivated by this historical approach, we neglect V–V–T exchange effects. We believe such consideration is worthy of further investigation and will investigate the limitations of this assumption in a future work.

3.3. *Vibrationally informed chemical reactions*

The influence of vibrational non-equilibrium on chemical reactions is based on the concept that chemical reactions are sensitive to the vibrational state, specifically that high-lying vibrational states tend to enhance reaction rates (Hammerling *et al.* 1959). If such high-lying states are over- or under-populated, the subsequent rate will increase or decrease, respectively. In other words, when $T_{v,i} > T_{tr}$ (vibrationally hot), high-lying states are more populated compared with the corresponding distribution at T_{tr}, so the reaction rate should increase compared with when $T_{v,i} = T_{tr}$. Likewise, when $T_{v,i} < T_{tr}$ (vibrationally cold), the rate should be suppressed. To model this effect, we build upon several historical modelling paradigms to develop a chemically–vibrationally consistent model for general, reversible reactions.

The molar production rates are calculated for J reversible reactions of the form

$$\sum_{i=1}^{N} \nu'_{ij}\chi_i \rightleftharpoons \sum_{i=1}^{N} \nu''_{ij}\chi_i, \tag{3.6}$$

where ν'_{ij} and ν''_{ij} are the species forward and reverse stoichiometric coefficients, respectively, and χ_i denotes the species (e.g. H_2). The species molar production rate is given by

$$\dot{\omega}_i = \sum_{j=1}^{J} \nu_{ij}\left(\Lambda_{f,j} - \Lambda_{r,j}\right), \quad \Lambda_{f,j} = k_{f,j} \cdot \prod_{i=1}^{N} c_i^{\nu'_{ij}}, \quad \Lambda_{r,j} = k_{r,j} \cdot \prod_{i=1}^{N} c_i^{\nu''_{ij}}, \tag{3.7}$$

where $\nu_{ij} = \nu''_{ij} - \nu'_{ij}$ is the net stoichiometric coefficient matrix and $\Lambda_{f,j}$ and $\Lambda_{r,j}$ are the forward and reverse reaction rates, respectively. Together, these represent the bulk (state-averaged) rate of change of the species mole fractions and account for all the quantised vibrational states of both the reactants and products. Also, $k_{f,j}$ and $k_{r,j}$ are the forward and reverse rate constants, respectively, and $c_i = \rho Y_i / W_i$ is the species concentration. We choose to model the rate constants using a vibrational efficiency function formulation (Hammerling *et al.* 1959; Treanor & Marrone 1962; Knab *et al.* 1995), i.e.

$$k_{f,j} = k^{eq}_{f,j}(T_{tr})\, \Phi_f(T_{tr}, \boldsymbol{T_v}), \quad k_{r,j} = k^{eq}_{r,j}(T_{tr})\, \Phi_r(T_{tr}, \boldsymbol{T_v}), \tag{3.8}$$

where $k^{eq}_{f,j}$ and $k^{eq}_{r,j}$ are the forward and reverse rate constants associated with thermal equilibrium, respectively, and Φ_f and Φ_r are the forward and reverse vibrational

https://doi.org/10.1017/jfm.2026.12034 Published online by Cambridge University Press

efficiency functions, respectively, which modify the rate to reflect the role of vibrational non-equilibrium. Here, $\boldsymbol{T_v}$ denotes the set of vibrational temperatures associated with the system.

Ideally, the efficiency function would be calculated directly via quantum calculations or QCT methods (Voelkel *et al.* 2016*a*). However, this approach remains computationally prohibitive for many relevant reactions when using quantum-level methods, and the generation of the realistic potential energy surfaces necessary for QCT calculations is often laborious and artisanal in nature; for example, a realistic potential energy surface for $N_2 + O_2$ requires over 2000 independent coefficients (Varga *et al.* 2016). With this in mind, we look to derive a generalised formulation for the vibrational efficiency function.

3.3.1. *Vibrational efficiency function formulation*

The vibrational efficiency function can be derived from the state-specific description of a reaction, given by

$$\sum_{i\in A} \chi_i(v_i) \rightleftharpoons \sum_{i\in B} \chi_i(w_i), \tag{3.9}$$

where A and B are the set of reactant and product species, respectively, and v_i and w_i are the corresponding vibrational states of the reactant and product species, respectively (v_i and w_i may be scalars or vectors depending on the species' vibrational degrees of freedom). Here, we utilise A (and B) rather than N to allow for repeat reactants (and products), with each having their own unique vibrational state. Also, we have dropped reaction-specific notation (the j subscript) in this section for brevity. Finally, we assume that this formulation is only vibrationally state-specific, and translational–rotational states are still characterised by T_{tr}.

The state-specific forward reaction rate is given by

$$\widetilde{\Lambda}_f(\boldsymbol{v}, \boldsymbol{w}) = c_A\, \widetilde{f}_A(\boldsymbol{v})\, \widetilde{k}_f(\boldsymbol{v}, \boldsymbol{w}), \tag{3.10}$$

where $c_A = \prod_{i\in A} c_i$ is the product of species concentrations, $\widetilde{f}_A(\boldsymbol{v}) = \prod_{i\in A} \widetilde{f}_{v,i}(v_i)$ is the product of reactant vibrational PDFs evaluated at $T_{v,i}$ (as described in § 2.1) and $\widetilde{k}_f(\boldsymbol{v}, \boldsymbol{w})$ is the state-specific rate constant. As before, the $\widetilde{\cdot}$ notation denotes that the quantity is state-specific, i.e. dependent on the vibrational state, and $\boldsymbol{v}$ and $\boldsymbol{w}$ are the set of reactant and product vibrational states, respectively. In general, we assume all quantities depend on both T_{tr} and $\boldsymbol{T_v}$, with different notation used to indicate non-standard temperature dependence. We define the state-specific rate constant as

$$\widetilde{k}_f(\boldsymbol{v}, \boldsymbol{w}) = k_f^{eq}\, \widetilde{\Phi}_f(\boldsymbol{v}, \boldsymbol{w}), \tag{3.11}$$

where k_f^{eq} is the rate constant assuming thermal equilibrium (evaluated at T_{tr}) and $\widetilde{\Phi}_f(\boldsymbol{v}, \boldsymbol{w})$ is the state-specific vibrational efficiency function. The state-averaged forward reaction rate, rate constant and vibrational efficiency function are defined by summing over the vibrational states, giving

$$\Lambda_f = c_A\, k_f, \quad k_f = k_f^{eq}\, \Phi_f, \quad \Phi_f = \sum_{\boldsymbol{v},\boldsymbol{w}} \widetilde{f}_A(\boldsymbol{v})\, \widetilde{\Phi}_f(\boldsymbol{v}, \boldsymbol{w}), \tag{3.12}$$

which is consistent with (3.7) and (3.8). Here, the summation over $\boldsymbol{v}$ includes all reactant vibrational states and corresponds to an average sum weighted by the vibrational partition function, and the summation over $\boldsymbol{w}$ includes all product vibrational states. Similar relations hold for the reverse rate, Λ_r, as derived from a corresponding state-specific rate constant, $\widetilde{k}_r(\boldsymbol{v}, \boldsymbol{w})$, and vibrational efficiency function, $\widetilde{\Phi}_r(\boldsymbol{v}, \boldsymbol{w})$.

https://doi.org/10.1017/jfm.2026.12034 Published online by Cambridge University Press

For reversible reactions, it is important for the vibrationally informed model to be consistent with the idea of an equilibrium constant, i.e. balance of the forward and reverse rates. Thus, the state-specific efficiency function is now constrained to ensure consistency under detailed balance via the following relation:

$$\widetilde{f}_A^*(\boldsymbol{v})\,\widetilde{k}_f(\boldsymbol{v},\boldsymbol{w}) = \mathcal{T}\,\widetilde{f}_B^*(\boldsymbol{w})\,\widetilde{k}_r(\boldsymbol{v},\boldsymbol{w}), \tag{3.13}$$

where $\widetilde{f}_A^*(\boldsymbol{v})$ and $\widetilde{f}_B^*(\boldsymbol{w})$ are the products of the reactant and product vibrational PDFs evaluated at some temperature, T_*, respectively. Summing over all vibrational states defines $\mathcal{T} = K_c^{eq}\,\Phi_f^*/\Phi_r^*$, where $K_c^{eq} = k_f^{eq}/k_r^{eq}$ is the equilibrium constant associated with thermal equilibrium, $\Phi_f^* = \sum_{\boldsymbol{v},\boldsymbol{w}} \widetilde{f}_A^*(\boldsymbol{v})\,\widetilde{\Phi}_f(\boldsymbol{v},\boldsymbol{w})$ and $\Phi_r^* = \sum_{\boldsymbol{v},\boldsymbol{w}} \widetilde{f}_B^*(\boldsymbol{w})\,\widetilde{\Phi}_r(\boldsymbol{v},\boldsymbol{w})$. Now, summing (3.13) over $\boldsymbol{v}$ results in the following relation:

$$\frac{\sum_{\boldsymbol{v}} \widetilde{f}_A^*(\boldsymbol{v})\,\widetilde{\Phi}_f(\boldsymbol{v},\boldsymbol{w})}{\Phi_f^*} = \frac{\sum_{\boldsymbol{v}} \widetilde{f}_B^*(\boldsymbol{w})\,\widetilde{\Phi}_r(\boldsymbol{v},\boldsymbol{w})}{\Phi_r^*}, \tag{3.14}$$

which must hold for the vibrationally aware rate constant to be consistent.

One approach to guarantee that (3.14) is satisfied is to assume that $\widetilde{\Phi}_f$ and $\widetilde{\Phi}_r$ are separable as follows:

$$\widetilde{\Phi}_f(\boldsymbol{v},\boldsymbol{w}) = a_f\,\widetilde{\omega}_f(\boldsymbol{v})\,\widetilde{s}_f(\boldsymbol{w}), \qquad \widetilde{\Phi}_r(\boldsymbol{v},\boldsymbol{w}) = a_r\,\widetilde{\omega}_r(\boldsymbol{w})\,\widetilde{s}_r(\boldsymbol{v}), \tag{3.15}$$

where a_f and a_r are functions of T_{tr}, defined to ensure consistency at thermal equilibrium; $\widetilde{\omega}_f(\boldsymbol{v})$ and $\widetilde{\omega}_r(\boldsymbol{w})$ are the forward and reverse efficiency scaling functions that determine how the reacting molecule's vibrational state enhances the rate; and $\widetilde{s}_f(\boldsymbol{w})$ and $\widetilde{s}_r(\boldsymbol{v})$ are functions to be defined based on the detailed balance constraint (3.14). Substituting this form into (3.14) and rearranging gives

$$\frac{\widetilde{s}_f(\boldsymbol{w})}{\sum_{\boldsymbol{w}} \widetilde{s}_f(\boldsymbol{w})} = \frac{\widetilde{f}_B^*(\boldsymbol{w})\,\widetilde{\omega}_r(\boldsymbol{w})}{\sum_{\boldsymbol{w}} \widetilde{f}_B^*(\boldsymbol{w})\,\widetilde{\omega}_r(\boldsymbol{w})}. \tag{3.16}$$

A sufficient constraint to ensure this relation holds is to set $\widetilde{s}_f(\boldsymbol{w}) = \widetilde{f}_B^*(\boldsymbol{w})\,\widetilde{\omega}_r(\boldsymbol{w})$. Following the same logic with (3.13), but summing over $\boldsymbol{w}$ instead of $\boldsymbol{v}$, results in a similar constraint for $\widetilde{s}_r(\boldsymbol{w})$.

The subsequent state-averaged vibrational efficiency functions, with a_f and a_r defined to ensure $\Phi_f = \Phi_r = 1$ at thermal equilibrium, are given by

$$\Phi_f = \frac{\Omega_f\,\Omega_r^*}{\Omega_f^{tr}\,\Omega_r^{tr}}, \qquad \Phi_r = \frac{\Omega_r\,\Omega_f^*}{\Omega_r^{tr}\,\Omega_f^{tr}}, \tag{3.17}$$

where

$$\begin{aligned}
&\Omega_f = \sum_{\boldsymbol{v}} \widetilde{f}_A(\boldsymbol{v})\,\widetilde{\omega}_f(\boldsymbol{v}), \quad \Omega_f^* = \sum_{\boldsymbol{v}} \widetilde{f}_A^*(\boldsymbol{v})\,\widetilde{\omega}_f(\boldsymbol{v}), \quad \Omega_f^{tr} = \sum_{\boldsymbol{v}} \widetilde{f}_A^{tr}(\boldsymbol{v})\,\widetilde{\omega}_f^{tr}(\boldsymbol{v}),\\
&\Omega_r = \sum_{\boldsymbol{w}} \widetilde{f}_B(\boldsymbol{w})\,\widetilde{\omega}_r(\boldsymbol{w}), \quad \Omega_r^* = \sum_{\boldsymbol{w}} \widetilde{f}_B^*(\boldsymbol{w})\,\widetilde{\omega}_r(\boldsymbol{w}), \quad \Omega_r^{tr} = \sum_{\boldsymbol{w}} \widetilde{f}_B^{tr}(\boldsymbol{w})\,\widetilde{\omega}_r^{tr}(\boldsymbol{w}),
\end{aligned} \tag{3.18}$$

and where the tr superscript denotes that the quantity is to be evaluated with all temperatures set to T_{tr}. Any choice for T_* is valid, but we choose to set $T_* = T_{tr}$, which is similar to the convention established by Knab *et al.* (1995). It follows that if $\widetilde{\omega}_r(\boldsymbol{w})$ is independent of $T_{v,i}$, then $\Omega_f^* = \Omega_f^{tr}$, and $\Phi_f = \Omega_f/\Omega_f^{tr}$ is only dependent on the reactant state (with a similar result for the reverse reaction). In general, we do not enforce any

https://doi.org/10.1017/jfm.2026.12034 Published online by Cambridge University Press

specific temperature dependencies on $\widetilde{\omega}_r(\boldsymbol{w})$, and instead look to define a generalised scaling function for a broad range of systems.

3.3.2. *A generalised vibrational scaling function*

The state-specific vibrational scaling function, $\widetilde{\omega}_f(\boldsymbol{v})$, controls how vibrational energy enhances the reaction rate. The only specific guideline for defining this function is that high-lying states tend to increase the reaction rate, the effect of which lessens as T_{tr} increases (Voelkel *et al.* 2016*b*). With this in mind, and motivated by historical precedent (as discussed below) (Marrone & Treanor 1963; Knab *et al.* 1995; Arsentiev *et al.* 2012; Voelkel *et al.* 2016*b*), we choose a form given by

$$\widetilde{\omega}_f(\boldsymbol{v}) = \prod_{i\in A} \exp\left(\frac{\widetilde{\varepsilon}_{v,i}(v_i)}{U_i}\right) \cdot \exp\left(\frac{\widetilde{\mathcal{E}}_{v,f}(\boldsymbol{v})}{T_{tr}}\right), \tag{3.19}$$

where $\widetilde{\varepsilon}_{v,i}(v_i)$ is the state-specific vibrational energy, normalised such that its units are temperature; U_i is a model parameter that determines how the collisional cross-section of the species increases with increasing vibrational energy (Marrone & Treanor 1963); and $\widetilde{\mathcal{E}}_{v,f}(\boldsymbol{v})$ is the effective vibrational component of the reaction barrier. Again, in this section, we forgo reaction-specific notation for brevity, but recognise that each of these parameters may depend on both species and reaction. The effective vibrational component $\widetilde{\mathcal{E}}_{v,f}(\boldsymbol{v})$ is defined to be a weighted sum given by

$$\widetilde{\mathcal{E}}_{v,f}(\boldsymbol{v}) = \sum_{\boldsymbol{w}} \widetilde{f}_B(\boldsymbol{w})\, \widetilde{\mathcal{E}}_{v,f}(\boldsymbol{v}, \boldsymbol{w}), \tag{3.20a}$$

$$\widetilde{\mathcal{E}}_{v,f}(\boldsymbol{v}, \boldsymbol{w}) = \sum_{i\in A} \alpha_{v,i}\, \widetilde{\varepsilon}_{v,i}(v_i) - \delta' \max\left[0,\ \widetilde{\Delta}_f(\boldsymbol{v}) - \delta'' \max\left(0,\ \widetilde{\Delta}_r(\boldsymbol{w})\right)\right], \tag{3.20b}$$

$$\widetilde{\Delta}_f(\boldsymbol{v}) = \sum_{i\in A} \alpha_{v,i}\, \widetilde{\varepsilon}_{v,i}(v_i) - \beta_f\, \mathcal{E}_{a,f},\ \ \widetilde{\Delta}_r(\boldsymbol{w}) = \sum_{i\in B} \alpha_{v,i}\, \widetilde{\varepsilon}_{v,i}(w_i) - \beta_r\, \mathcal{E}_{a,r}, \tag{3.20c}$$

where $\alpha_{v,i}$ is the vibrational efficiency parameter; β_f and β_r are parameters that scale forward and reverse activation energies, respectively; $\mathcal{E}_{a,f}$ and $\mathcal{E}_{a,r}$ are the forward and reverse activation energies in temperature units, respectively; and δ' and δ'' are constants equal to either zero or one. The effective vibrational component $\widetilde{\mathcal{E}}_{v,f}(\boldsymbol{v})$ is defined so that vibrational energies above the forward activation energy are limited to the forward activation energy, which itself may increase for sufficiently large product vibrational energies greater than the reverse activation energy. For this generalised model, we assume that each of these parameters may have some temperature dependency. A corresponding form for the reverse efficiency scaling function $\widetilde{\omega}_r(\boldsymbol{w})$ can also be defined.

The motivation for the effective vibrational component of the reaction barrier, $\widetilde{\mathcal{E}}_{v,f}(\boldsymbol{v})$, is based on a simplified reaction pathway illustrated in figure 1. Here, we show how a reference reaction path (black line), defined assuming the vibrational contributions of reactant and product species are zero, is modified by the reactant and product vibrational energies (red line). In short, the reactant vibrational energy reduces the translational–rotational energy needed for reaction; as such, higher vibrational energy in the reactants leads to increased reaction rates. Here, we define the magnitude of that increase by $\sum_{i\in A} \alpha_{v,i}\widetilde{\varepsilon}_{v,i}(v_i)$, limited by the reference activation energy barrier as defined in (3.20). The vibrational energy efficiency parameter, $\alpha_{v,i}$, controls how effective the vibrational energy is at contributing to the activation energy. Here, $\alpha_{v,i}$ is intended to be a representative value associated with each chemical species, independent of its

https://doi.org/10.1017/jfm.2026.12034 Published online by Cambridge University Press

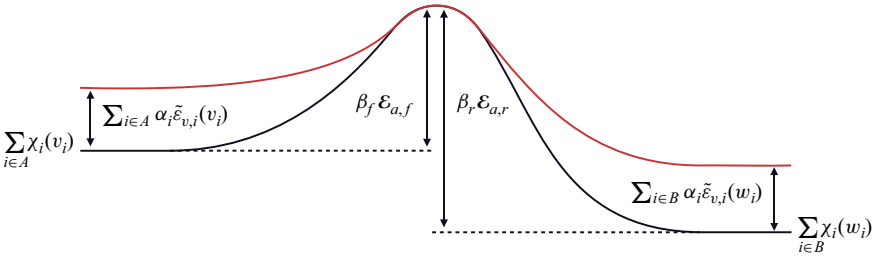


Figure 1. A simplified reaction path diagram. The black line illustrates a reference reaction pathway assuming negligible vibrational energy contributions, and the red line shows how the path shifts as the reactant and product vibrational energies increase.

complexity (e.g. number of vibrational modes). In our analysis, because we have assumed that intramolecular vibrational relaxation is instantaneous (resulting in one vibrational temperature per species), we observe that a set of vibrational mode-specific efficiency parameters does not materially alter the modelling flexibility granted by assigning a single, representative value. The activation energies $\mathcal{E}_{a,f}$ and $\mathcal{E}_{a,r}$ are scaled by β_f and β_r, respectively, to account for the notion that the reference path assumes no contributions from vibrational energy, though $\mathcal{E}_{a,f}$ and $\mathcal{E}_{a,r}$ are determined independently of this assumption.

Several historical models can be reconstructed using this general model. Setting parameters so that $\widetilde{\mathcal{E}}_{v,f}(\boldsymbol{v}) = \widetilde{\mathcal{E}}_{v,r}(\boldsymbol{w}) = 0$ recovers the model presented by Marrone & Treanor (1963). Under this model, the efficiency function only varies with respect to U_i, so the increased cross-section of reactants with high-lying vibrational states is accounted for, but the vibrational energy has no effect on the reaction barrier. Setting $\delta'' = 0$ recovers the CVCV model (Knab *et al.* 1995), though the original model did not include $\alpha_{v,i}$ (the α parameter from the original paper is replaced by β_f in this formulation). Under this model, the reverse activation energy does not contribute to the modified reaction barrier. This neglects products with high-lying vibrational states greater than the reverse reaction barrier, thus potentially cutting off vibrational states that could enhance the rate. Setting $U_i = \infty$ recovers a model motivated by Arsentiev *et al.* (2012). However, the original model did not impose an assumption that the efficiency function is separable into reactant and product states, resulting in a non-separable state-specific efficiency function, with $\widetilde{\Phi}_f(\boldsymbol{v}, \boldsymbol{w}) \sim \exp(\widetilde{\mathcal{E}}_{v,f}(\boldsymbol{v}, \boldsymbol{w})/T_{tr})$. For general reactions, it is unclear how the approach by Arsentiev *et al.* (2012) affects the detailed balance of reversible reactions. Finally, setting $U_i = \infty$ and $\alpha_{v,i} = 0.6 - T_{tr}/10^4$ recovers a model similar to that presented by Voelkel *et al.* (2016*b*), though this model had a slightly different approach for handling the reference energy barrier.

3.4. *Chemical–vibrational energy exchange*

Chemical–vibrational energy exchange represents the creation and destruction of vibrational energy from chemical reactions. For a state-specific rate as defined in § 3.3.1, the destruction of energy at a particular vibrational state is determined by the forward rate multiplied by the energy associated with that state (Knab *et al.* 1995). A similar definition applies for the creation of energy as determined via the reverse rate. A weighted average over the state-specific creation and destruction of energy results in the bulk C–V exchange.

https://doi.org/10.1017/jfm.2026.12034 Published online by Cambridge University Press

Thus, for a given reaction, j, the C–V exchange rate for a reactant species is given by

$$\frac{S_{C-V,ij}}{W_i} = c_{B,j} \sum_{\boldsymbol{v},\boldsymbol{w}} \widetilde{f}_B(\boldsymbol{w})\, \widetilde{k}_{r,j}(\boldsymbol{v},\boldsymbol{w})\, \widetilde{e}_{v,i}(v_i) - c_{A,j} \sum_{\boldsymbol{v},\boldsymbol{w}} \widetilde{f}_A(\boldsymbol{v})\, \widetilde{k}_{f,j}(\boldsymbol{v},\boldsymbol{w})\, \widetilde{e}_{v,i}(v_i), \tag{3.21}$$

where $\widetilde{e}_{v,i}(v_i) = R_i\, \widetilde{\varepsilon}_{v,i}(v_i)$ is the state-specific vibrational energy per unit mass. A similar relation holds for product species. Accounting for generalised reactant and product combinations, and multiple reactions, the resulting state-averaged C–V exchange rate becomes

$$S_{C-V,i} = \sum_{j=1}^{J} S_{C-V,ij},$$

$$S_{C-V,ij} = W_i \Lambda_{r,j} \left(\nu'_{ij}\, G^*_{f,ij} - \nu''_{ij}\, G_{r,ij} \right) - W_i \Lambda_{f,j} \left(\nu'_{ij}\, G_{f,ij} - \nu''_{ij}\, G^*_{r,ij} \right), \tag{3.22}$$

where

$$G_{f,ij} = \sum_{\boldsymbol{v}} \widetilde{f}_A(\boldsymbol{v})\, \widetilde{\omega}_{f,j}(\boldsymbol{v})\, \widetilde{e}_{v,i}(v_i)/\Omega_{f,j}, \quad G^*_{f,ij} = \sum_{\boldsymbol{v}} \widetilde{f}^*_A(\boldsymbol{v})\, \widetilde{\omega}_{f,j}(\boldsymbol{v})\, \widetilde{e}_{v,i}(v_i)/\Omega^*_{f,j},$$
$$G_{r,ij} = \sum_{\boldsymbol{w}} \widetilde{f}_B(\boldsymbol{w})\, \widetilde{\omega}_{r,j}(\boldsymbol{w})\, \widetilde{e}_{v,i}(w_i)/\Omega_{r,j}, \quad G^*_{r,ij} = \sum_{\boldsymbol{w}} \widetilde{f}^*_B(\boldsymbol{w})\, \widetilde{\omega}_{r,j}(\boldsymbol{w})\, \widetilde{e}_{v,i}(w_i)/\Omega^*_{r,j}. \tag{3.23}$$

Physically, $G^*_{f,ij}$ and $G^*_{r,ij}$ quantify the production of vibrational energy from reactions, whereas $G_{f,ij}$ and $G_{r,ij}$ quantify the destruction of vibrational energy.

4. Proposed model for high-speed combustion

The governing equations and constitutive relations described in §§ 2 and 3 represent a general framework for modelling vibrational non-equilibrium flows. The main assumptions are as follows. First, we assume that the bulk vibrational energy of each species can be characterised by a single, species-specific temperature. The vibrational energy is transported independently of the total energy, with relaxation and redistribution modelled via T–V and V–V exchange, respectively, and with V–V–T neglected. Additionally, chemical reactions produce or destroy vibrational energy based on a vibrationally informed reaction mechanism, the underlying assumptions of which are (1) that the state-specific non-equilibrium reaction rate is equivalent to the equilibrium reaction rate scaled by some state-specific vibrational efficiency function, (2) that the efficiency function is separable into reactant and product contributions and (3) that vibrational hot (or cold) species enhance (or suppress) the reaction rate.

The resulting model follows naturally from these assumptions, with the following parameters needed to close the system:

$$P_{T-V,ij}, \quad P_{V-V,ij}, \quad \alpha_{v,ij}. \tag{4.1}$$

For a typical hydrogen–air mixture with 9 species, 7 of which are non-monatomic, and 20 reactions, this corresponds to more than 200 free parameters to define. To further complicate this situation, we expect each parameter to exhibit some level of dependence on T_{tr}, resulting in even more parameters to define. In general, these parameters can be defined independently in isolation or collectively as a calibration based on complex reacting flow experiments. When calibrating each parameter in isolation, a number of numerical and experimental techniques can be employed. For instance, one could

https://doi.org/10.1017/jfm.2026.12034 Published online by Cambridge University Press

calculate state-specific exchange and reaction probabilities from numerical studies based on first principles (e.g. from QCT analysis). However, as noted in § 3.3, generating state-specific exchange and reaction probabilities is limited to relatively simple binary mixtures. Thus, rather than calculating the exchange probabilities and efficiency parameter directly from state-specific studies, a smaller subset of studies could instead be used to inform a correlation that is applicable within the regime of interest based on the molecular properties of each species.

Another approach could be to calibrate these parameters based on empirical shock tube and detonation measurements. For exchange mechanisms, many studies have looked at a wide range of species pairwise interactions, but depending on the application and chemical mechanism, data gaps undoubtedly exist. As with state-specific studies, though, a relatively small subset of data could be used to establish a correlation for a wide range of species. For vibrational efficiency, isolating and extracting data become far more difficult because vibrational non-equilibrium is inherently present within the measurements. Thus, even if we account for the coupled relaxation process leading up to the measurement, we still have to contend with isolating the non-equilibrium contribution related to that measurement.

Ideally, as long as these parameters are set to reasonable values, we expect the model to recover physically consistent behaviours that we expect in vibrational non-equilibrium flow fields. In the end, we leverage each of these approaches depending on the application, desired accuracy and feasibility. Correlations are sufficient for some processes, while others can be informed by empirical measurements, and still others may be calculated directly from state-specific formulations. To show this approach in practice, we now demonstrate how to apply this framework to a specific application space and temperature regime, namely high-speed combustion flows with temperatures below 5000 K, including supersonic combustion and typical detonation conditions.

4.1. *Vibrational partitioning of the internal energy*

For high-speed combustion applications, complex chemical mechanisms are typically developed under the assumption of a specific equation of state. For instance, the hydrogen–air chemical mechanism presented by Burke *et al.* (2012) supports both thermodynamic state and molar production rate calculations via Chemkin-II (Kee *et al.* 1989). The associated equation of state is the NASA 7-coefficient polynomial model. Modifying the equation of state to, say, a rigid-rotor harmonic oscillator model would necessitate recalibration of the kinetic mechanism. With this in mind, we will assume that the internal energy (at thermal equilibrium) is defined via some functional form, denoted by e_i^{fit}. Because we will eventually need the vibrational partition function for each species to define the vibrational efficiency function (see (4.7) below), we choose to define vibrational energy explicitly via the harmonic oscillator approximation and calculate the translational–rotational energy implicitly. Thus, the species internal energy as defined in (2.5) has translational–rotational and vibrational components given by

$$e_{tr,i}(T_{tr}) = e_i^{fit}(T_{tr}) - e_{v,i}(T_{tr}), \quad e_{v,i}(T_{v,i}) = \sum_{j=1}^{N_{v,i}} \frac{R_i \theta_{v,ij}}{\mathrm{e}^{\theta_{v,ij}/T_{v,i}} - 1}, \tag{4.2}$$

where $N_{v,i}$ is the vibrational degrees of freedom and $\theta_{v,ij}$ is the characteristic vibrational temperature corresponding to the species' jth vibrational mode. For a species with $N_{a,i}$ atoms, $N_{v,i} = 0$ if the species is monatomic ($N_{a,i} = 1$), $N_{v,i} = 3N_{a,i} - 5$ if the species is linear and $N_{v,i} = 3N_{a,i} - 6$ if the species is nonlinear.

https://doi.org/10.1017/jfm.2026.12034 Published online by Cambridge University Press

Several other relatively simple options could be used to define the vibrational energy. First, we could employ an anharmonic oscillator model or truncated harmonic oscillator model and replace $e_{v,i}$ in (4.2) accordingly. Section 5.1 explores both of these choices with regard to the vibrational efficiency function. Second, for complex molecules, where characteristic vibrational temperatures are not fully defined, it may be preferred to define the translational–rotational–electronic energy explicitly (via a rigid-rotor approximation, for instance) and calculate the vibrational energy implicitly from e_i^{fit}. Under this formulation, the vibrational partition function is calculated by integrating (2.4). Because we are calculating the vibrational energy implicitly, extra care must be taken to ensure that the vibrational energy and partition function are physically consistent (e.g. $e_{v,i} > 0$, $\mathrm{d}e_{v,i}/\mathrm{d}T_{v,i} > 0$, $\mathrm{d}Q_{v,i}/\mathrm{d}T_{v,i} > 0$, etc.).

4.2. *Translational–vibrational exchange*

To fully specify T–V exchange, the pairwise T–V relaxation time scale, $\tau_{T-V,ij}$, must be defined. Ideally, the time scale for each species' pairwise combination could be individually calculated or measured. The literature provides an abundance of such studies, though they are typically focused on a relatively limited set of species' pairwise interactions. For a wide range of diatomic molecules, Millikan & White (1963) showed that the following correlation generally agrees to within 50 % of the empirical measurements:

$$p \cdot \tau_{T-V,ij} = \exp\left[A W_{ij}^{1/2} \theta_{v,i}^{4/3} \left(T_{tr}^{-1/3} - B W_{ij}^{1/4}\right) - C\right], \tag{4.3}$$

where $A = 1.16 \times 10^{-3}$, $B = 1.50 \times 10^{-2}$ and $C = 18.42$ are constants determined via calibration; and W_{ij} is the reduced mass of the colliding pair. The units of A, B and C are defined assuming W_{ij} is in $\mathrm{g\,mol^{-1}}$ and T_{tr} and $\theta_{v,ij}$ are in K. The corresponding T–V exchange probability is given by $P_{T-V,ij} = \tau_{c,ij}/\tau_{T-V,ij}$, where $\tau_{c,ij}$ is defined in (3.2). Many other choices for the T–V relaxation time scale have been proposed, including corrections for high temperatures (Park 1989). For temperatures below 10 000 K, these high-temperature corrections have negligible impact on the relaxation time scale (see figure 7.3 in Boyd & Schwartzentruber (2017)). The Millikan & White model is included here and used in the subsequent analysis due to its historical significance and to provide a general understanding of the approximate time scales in detonations.

4.3. *Vibrational–vibrational exchange*

The key parameters in defining V–V exchange are the collision cross-section, σ_{ij}, which controls the collision time scale via (3.2), and the exchange probability, $P_{V-V,ij}$. The collision cross-section is a measure of area that describes the propensity of two molecules to affect one another's trajectory via a collision. The value for σ_{ij} can be calculated via QCT methods, which may employ a potential energy surface determined from quantum chemistry computations, or from some intermolecular potential, such as a hard-sphere potential, inverse power-law potential or Lennard-Jones potential (Boyd & Schwartzentruber 2017). The hard-sphere model represents the simplest such model, with $\sigma_{ij} = \pi d_{ij}^2$, where d_{ij} is the average diameter of the species pair. The challenge remains to determine this 'diameter' for each species. In general, the hard-sphere model can be used to calculate transport properties such as viscosity, which is approximately $5(2\pi W_i \mathcal{R}_u T)^{1/2}/(16\pi \mathcal{N}_A d_i)$, where d_i is the species diameter (Boyd & Schwartzentruber 2017). With viscosity measurements from Lemmon *et al.* (2024), such a relation allows us to approximate the diameter for a range of molecules. For hydrogen–air mixtures below 5000 K, the calculated hard-sphere diameters range between 2 and 4 Å. Due to the complex

https://doi.org/10.1017/jfm.2026.12034 Published online by Cambridge University Press

nature of calculating the collision cross-section and the limited accuracy of the hard-sphere approximation itself, we set d_{ij} to an average value of 3 Å for each collision pair.

With regard to the exchange probability, $P_{V-V,ij}$ is typically set as a constant value depending on the system (Candler & MacCormack 1988, 1991; Knab *et al.* 1992, 1995; Voelkel *et al.* 2016*a*). However, such an assumption is inconsistent with the thermal equilibrium constraint described by (3.4) because $P_{V-V,ij}$ is not necessarily symmetric. Consider that if we assume $P_{V-V,ij}$ is symmetric, then (3.4) is valid if and only if $\mathrm{e}_{v,i}^{tr} = e_{v,j}^{tr}$, which itself is only valid under rare conditions. By invalidating (3.4), then $\sum_i S_{V-V,i}/W_i$, with $S_{V-V,i}$ defined in (3.5), is not necessarily zero. However, $\sum_i S_{V-V,i}/W_i$ should be zero based on the base V–V exchange model as defined in (3.3). Thus, assuming $P_{V-V,ij}$ is symmetric inadvertently modifies how V–V exchange affects the translational–rotational energy, a process that we refer to as 'leakage' and one that we wish to avoid.

To rectify this inconsistency, we set $P_{V-V,ij}$ as follows:

$$P_{V-V,ij} = P'_{V-V,ij}\left(\frac{(e_{v,i}^{tr} + e_{v,j}^{tr})/2}{e_{v,i}^{tr}}\right), \tag{4.4}$$

where $P'_{V-V,ij}$ is a modified (symmetric) probability factor associated with species pairwise vibrational transfer. Setting $P'_{V-V,ij}$ to a constant value is now consistent with (3.4) and $S_{V-V,ij}/W_i = -S_{V-V,ji}/W_j$, thus ensuring that $\sum_i S_{V-V,i}/W_i = 0$. Our choice for $P_{V-V,ij}$ is motivated by (3.4), wherein $P_{V-V,ij}e_{v,i}^{tr}$ and $P_{V-V,ji}e_{v,j}^{tr}$ are expected to increase monotonically with T_{tr}. With $P_{V-V,ij}$ set to be proportional to the average species pairwise vibrational energy at thermal equilibrium, the left- and right-hand sides of (3.4) still increase monotonically with $P'_{V-V,ij}$ set to a constant value.

In general, we expect $P'_{V-V,ij}$ to be similar in magnitude to $P_{V-V,ij}$ and $P_{V-V,ji}$, so the previous historical reference values are still valid. Originally, $P_{V-V,ij}$ was set to a constant value of 10^{-2} (Candler & MacCormack 1988, 1991; Knab *et al.* 1992, 1995; Fiévet *et al.* 2017). This value seemed to be sufficient for high-speed reentry flows of interest in those studies. However, in measuring the vibrational–rotational relaxation process of N_2 and O_2 within high-speed turbulent diffusion flames, Reising *et al.* (2016) observed that a value closer to 10^{-5} provided the best match between simulations and experimental measurements. It is also well established that $P_{V-V,ij}$ is not only species-dependent, but also temperature-dependent. For instance, Taylor *et al.* (1967) measured V–V exchange probabilities between 10^{-4} and 10^{-3} for $NO - CO$, $NO - N_2$ and $CO_2 - N_2$ mixtures between 500 and 2000 K. Schwartz *et al.* (1952) predicted values between approximately 10^{-5} and 10^{-4} for $N_2 - O_2$ collisions. Voelkel (2016) directly calculated $N_2 - O_2$ scattering rates via QCT and determined that the V–V exchange probability varies between 10^{-6} and 10^{-4} for temperatures between 1000 and 3000 K. These collective observations were used to motivate a change from $P_{V-V,ij} = 10^{-2}$ to 10^{-4} for the numerical study by Voelkel *et al.* (2016*a*).

This breadth of studies demonstrates that the V–V exchange represents a complex, species-specific and temperature-dependent phenomenon, and that a robust model for the exchange probability is still a matter of considerable research. With this in mind, we explore a range of constant values for $P'_{V-V,ij}$ to provide a broad view of how V–V exchange works and couples with other vibrational exchange processes, and we look towards potential future studies for the development of a generalised, species- and temperature-dependent exchange probability model.

https://doi.org/10.1017/jfm.2026.12034 Published online by Cambridge University Press

4.4. *Vibrationally informed chemical reactions*

For modelling vibrationally-informed chemical reactions, it remains to define the model parameters associated with our form of the vibrational scaling function (3.19), which in turn defines the vibrational efficiency function (3.17). Under high-speed combustion conditions, where temperatures are typically below 5000 K, we assume vibrational energies exceeding the reaction activation energy are negligible in the flow. This is equivalent to setting $\delta' = 0$ in (3.20). The resulting effective vibrational component of the reaction barrier reduces to $\widetilde{\mathcal{E}}_{v,f}(\boldsymbol{v}) = \sum_{i\in A} \alpha_{v,i}\, \widetilde{\varepsilon}_{v,i}(v_i)$, and the state-specific vibrational scaling function as defined in (3.19) becomes

$$\widetilde{\omega}_f(\boldsymbol{v}) = \prod_{i\in A} \exp\left[\widetilde{\varepsilon}_{v,i}(v_i)\left(\frac{\alpha_{v,i}}{T_{tr}} + \frac{1}{U_i}\right)\right]. \tag{4.5}$$

Recognising that $\widetilde{f}_A(\boldsymbol{v}) = \prod_{i\in A} \widetilde{f}_{v,i}(v_i)$ and $\widetilde{f}_{v,i}(v_i) = \prod_{i\in A} \exp[-\widetilde{\varepsilon}_{v,i}(v_i)/T_{v,i}]/Q(T_{v,i})$, where $Q_{v,i}$ is the vibrational partition function as described in § 2.1, then Ω_f and Ω_f^{tr} as defined in (3.18) reduce to

$$\Omega_f = \prod_{i\in A} \frac{Q_{v,i}(\Gamma_i)}{Q_{v,i}(T_{v,i})}, \quad \Omega_f^{tr} = \prod_{i\in A} \frac{Q_{v,i}(\Gamma_i^{tr})}{Q_{v,i}(T_{tr})}, \tag{4.6}$$

where $1/\Gamma_i = 1/T_{v,i} - \alpha_{v,i}/T_{tr} - 1/U_i$ and $1/\Gamma_i^{tr} = (1-\alpha_{v,i})/T_{tr} - 1/U_i$ are effective 'gamma' temperatures. Similar reductions exist for Ω_r and Ω_r^{tr}. The resulting efficiency function is given by

$$\Phi_{f,j} = \prod_{i=1}^{N} \varphi_i^{\nu'_{ij}}, \quad \Phi_{r,j} = \prod_{i=1}^{N} \varphi_i^{\nu''_{ij}}, \quad \varphi_i = \frac{Q_{v,i}(T_{tr})\, Q_{v,i}(\Gamma_i)}{Q_{v,i}(T_{v,i})\, Q_{v,i}(\Gamma_i^{tr})}, \tag{4.7}$$

where φ_i is the species efficiency function. Here, we have assumed $\alpha_{v,i}$ and U_i do not vary between reactions, resulting in a reaction-independent species vibrational efficiency function. The effective temperatures Γ_i and Γ_i^{tr} modulate the magnitude of the vibrational efficiency function's scaling behaviour depending on the value of $\alpha_{v,i}$ and U_i. Note that this model does not explicitly require a specific vibrational energy description, thus allowing for the use of harmonic, truncated harmonic and anharmonic oscillator models, as well as energy levels measured empirically or calculated directly from a potential energy surface, as long as the vibrational partition function is well defined.

For this vibrational efficiency function, we seek a model with the following physically consistent behaviour. For a given species denoted by i, with T_{tr} and $T_{v,k\neq i}$ fixed, a vibrationally cold state ($T_{v,i} < T_{tr}$) has under-excited high-lying vibrational modes and should reduce the reaction rate, whereas a vibrationally hot state ($T_{v,i} > T_{tr}$) has over-excited high-lying vibrational modes and should increase the reaction rate. Furthermore, the farther $T_{v,i}$ is from T_{tr}, the more pronounced this effect will become. To ensure this behaviour, we simply require that $\Phi_{f,j}$ increases monotonically with $T_{v,i}$ ($\partial\Phi_{f,j}/\partial T_{v,i} \geq 0$). We assume that the $Q_{v,i}$ is positive for physical (positive) temperatures, so it is sufficient to show that $\partial\varphi_i/\partial T_{v,i} \geq 0$ to satisfy the monotonicity condition.

This condition constrains the vibrational efficiency parameter, $\alpha_{v,i}$. For our implementation, which utilises the harmonic oscillator approximation, a sufficient constraint requires $\alpha_{v,i} \geq -T_{tr}/U_i$, as well as $\partial\alpha_{v,i}/\partial T_{v,i} \geq 0$ when $T_{v,i} < T_{tr}$ and $\partial\alpha_{v,i}/\partial T_{v,i} \leq 0$ when $T_{v,i} > T_{tr}$. Note that this is a sufficient constraint, with more relaxed constraints requiring a balance of $\partial\alpha_{v,i}/\partial T_{v,i}$ against a series of partition functions. This, in conjunction with a constraint requiring non-negative but finite gamma temperatures

https://doi.org/10.1017/jfm.2026.12034 Published online by Cambridge University Press

to ensure $0 \leq \Phi_{f,j} < \infty$, results in the following constraints on the vibrational efficiency parameter:

$$-\frac{T_{tr}}{U_i} \leq \alpha_{v,i} < \frac{1}{\max(\,1,\ T_{v,i}/T_{tr}\,)} - \frac{T_{tr}}{U_i}. \tag{4.8}$$

These bounds represent the minimum and maximum extent to which vibrational non-equilibrium can influence reaction kinetics. When $\alpha_{v,i} = -T_{tr}/U_i$, then $\Gamma_i = T_{v,i}$ and $\Phi_{f,j} = 1$, indicating no vibrational non-equilibrium effect. When $\alpha_{v,i} = 1/\max(1, T_{v,i}/T_{tr}) - T_{tr}/U_i - \delta$, where δ is a small perturbation, $\Gamma_i^{tr} = T_{tr}/\delta$ when $T_{v,i} < T_{tr}$ and the efficiency function goes to zero, while $\Gamma_i = T_{tr}/\delta$ when $T_{v,i} > T_{tr}$ and the efficiency function goes to infinity. Given these bounds, it is convenient to define $\alpha_{v,i}$ as some fractional value of the minimal and maximal vibrational effect, i.e.

$$\alpha_{v,i} = \frac{\alpha'_{v,i}}{\max(\,1,\ T_{v,i}/T_{tr}\,)} - \frac{T_{tr}}{U_i}, \tag{4.9}$$

where $\alpha'_{v,i} \in [0, 1)$ is the modified vibrational efficiency parameter. The resulting gamma temperatures are now independent of U_i, and only $\alpha'_{v,i}$ needs to be defined.

As a final note, we recognise that introducing a vibrational temperature into the definition for $\alpha_{v,i}$ should be addressed. Rather than evaluating $\alpha_{v,i}$ at T_{tr} when setting Γ_i^{tr}, we choose to maintain the vibrational temperature dependency. This choice does not alter the underlying formulation of Φ_f and Φ_r in (3.17) because the equilibrium limit is still recovered. Consider the alternative, whereby Γ_i^{tr} is evaluated using $\alpha_{v,i}^{tr}$ ($\alpha_{v,i}$ evaluated with $T_{v,i}$ set to T_{tr}). The subsequent constraints (assuming $U_i \to \infty$ for brevity) to ensure $\partial\varphi_i/\partial T_{v,i} \geq 0$ and positive gamma temperatures are $0 \leq \alpha_{v,i} < T_{tr}/T_{v,i}$, $0 \leq \alpha_{v,i}^{tr} < 1$ and $\partial\alpha_{v,i}/\partial T_{v,i} \geq -T_{tr}/T_{v,i}^2 \cdot Q(T_{v,i})/Q(T_{tr}/\alpha_{v,i})$ (or simply that $\partial\alpha_{v,i}/\partial T_{v,i} \geq 0$). It is straightforward to show that for vibrationally hot flows, $\alpha_{v,i}$ may potentially have to decrease to ensure $\alpha_{v,i} < T_{tr}/T_{v,i}$, otherwise Γ_i will be negative. However, as $\alpha_{v,i}$ decreases, the constraint for $\partial\alpha_{v,i}/\partial T_{v,i}$ will eventually be invalidated, resulting in $\partial\varphi_i/\partial T_{v,i} < 0$ (a rate that decreases as $T_{v,i}$ increases). It is this restriction that motivates our choice to simply evaluate Γ_i^{tr} at $\alpha_{v,i}$ (and maintain the vibrational temperature dependency).

4.5. *Chemical–vibrational exchange*

For the vibrational efficiency model described in § 4.4, the resulting species- and reaction-dependent C–V exchange rate as defined in (3.22) reduces to

$$S_{C-V,ij} = \rho Y_i e_{v,i}^{tr} \left(\frac{e_{v,i}(\Gamma_i^{tr})/e_{v,i}^{tr}}{\tau_{C-V(c),ij}} - \frac{e_{v,i}(\Gamma_i)/e_{v,i}^{tr}}{\tau_{C-V(d),ij}} \right), \tag{4.10}$$

where $\tau_{C-V(c),ij} = \rho Y_i/[W_i(\nu'_{ij}\Lambda_{r,j} + \nu''_{ij}\Lambda_{f,j})]$ and $\tau_{C-V(d),ij} = \rho Y_i/[W_i(\nu'_{ij}\Lambda_{f,j} + \nu''_{ij}\Lambda_{r,j})]$ are the C–V time scales for the creation (c) and destruction (d) of vibrational energy from chemical reactions. Here, we include the $\rho Y_i e_{v,i}^{tr}$ term to have C–V exchange in a similar form compared with T–V exchange via (3.1) and V–V exchange via (3.5). The corresponding C–V exchange time scale is proportional to the reaction time scales associated with the flow.

4.6. *Guidance on selecting parameter values*

Our proposed vibrational non-equilibrium model for high-speed combustion requires two sets of model parameters to close the system: $P'_{V-V,ij} > 0$ and $\alpha'_{v,i} \in [0, 1)$. For a typical

https://doi.org/10.1017/jfm.2026.12034 Published online by Cambridge University Press

hydrogen–air mixture with seven non-monatomic species, six of which are part of the reaction mechanism, then 21 $P'_{V-V,ij}$ and 6 $\alpha'_{v,i}$ values (or closures) are needed. Consider also that $P'_{V-V,ij}$ generally depends on T_{tr}. For instance, in V–V exchange collisions of N_2 and O_2, Voelkel (2016) found that for any fixed T_{tr} (below 3000 K), $P'_{V-V,ij}$ was approximately constant. However, for T_{tr} varied between 500 and 3000 K, the value of $P'_{V-V,ij}$ varied by approximately three orders of magnitude. These results suggest that a temperature dependence is likely warranted for predicting accurate relaxation phenomena. The same likely applies to $\alpha'_{v,i}$ (though using a different model, consider the discussion by Voelkel *et al.* (2016*a*)). It is also possible that a global model or correlation, akin to the T–V exchange time scale presented by Millikan & White (1963), could significantly reduce the number of new parameters needed to close the system by relying on basic molecular properties of each species and colliding pair.

All of this points to the need for a modern reassessment of the V–V exchange mechanism. Though beyond the scope of this work, we believe that collating and systematically examining historical V–V exchange studies could potentially reveal a global correlation valid within the high-speed combustion regime. However, we also recognise that legacy studies only offer a patchwork of rates, probabilities and behaviours associated with specific binary mixtures. Thus, part of this work would also necessarily entail identification of data gaps that need to be addressed, through either state-specific modelling efforts or new relaxation experiments.

Once the relaxation mechanism is determined, then $\alpha'_{v,i}$ can be addressed. Here, we would recommend two paths: (i) calculate state-specific reaction rates from studies motivated by first principles analysis, such as QCT-based methods, and (ii) calibrate $\alpha'_{v,i}$ to recover empirical measurements associated with combustion, including the induction zone length and unsteady behaviour (cellular structure) of detonation waves. The first approach will provide valuable insights into the nature of $\alpha'_{v,i}$, specifically regarding the assumptions of reaction independence and potential dependencies on T_{tr}. The second approach is more practical and recognises that complex chemical mechanisms are highly coupled systems and stem from a wide range of sources. Not every reaction can leverage QCT-based methods to evaluate $\alpha'_{v,i}$. Instead, we can set $\alpha'_{v,i}$ based on a smaller subset of studies to achieve specific behaviours, and then validate that choice by ensuring that the model accurately predicts specific empirical measurements and behaviours. Essentially, we treat $\alpha'_{v,i}$ as a reduced parametrisation and calibrate its value to recover important application-specific features, similar to other reduced modelling efforts (e.g. the chemical–diffusive model) (Lu *et al.* 2021).

Another approach, consistent with historical non-equilibrium studies (Candler & MacCormack 1988, 1991; Knab *et al.* 1995; Voelkel *et al.* 2016*a*), would be to further assume that $P'_{V-V,ij}$ and $\alpha'_{v,i}$ can be set to a constant value representing an average effect, thus necessitating only two parameter values to close the system. This is the choice we make in Part 2 (Voelkel *et al.* 2026) of this work to study the role of non-equilibrium within inert shocks and steady detonation waves of hydrogen–air mixtures. Therein, $P'_{V-V,ij}$ is set to a constant value, varied between 10^{-6} and 10^{-2}. Over this range, the relaxation dynamics shifts completely from no V–V effect (entirely dominated by T–V exchange) to being completely determined by the fastest-relaxing species in the mixture (species are 'pulled' towards equilibrium by the species with the greatest T–V exchange). A value of 10^{-4} is shown to provide a good balance of expected physical observations, namely that N_2 relaxation is significantly enhanced by H_2O, but this effect is lessened when N_2 is mixed with O_2.

https://doi.org/10.1017/jfm.2026.12034 Published online by Cambridge University Press

Likewise, $\alpha'_{v,i}$ is varied between a value of 0.0 and 0.8 in Part 2 (Voelkel *et al.* 2026), beyond which the induction zone length of steady detonations increases by a factor of more than 40 % (and increases exponentially as $\alpha'_{v,i}$ grows further). A value of 0.0 reduces the induction zone by nearly 20 %. In recommending a value for future studies, we first recognise that detailed chemical mechanisms are derived from shock tube and detonation experiments that can neither completely isolate nor completely remove vibrational non-equilibrium effects. Thus, non-equilibrium effects are inherently present in such measurements, which in turn are used to calibrate models that traditionally assume vibrational equilibrium. This introduces a physical inconsistency, in that an equilibrium model is calibrated to a flow field with non-equilibrium effects. Even so, the equilibrium model is calibrated to the measured data. It follows that the non-equilibrium results should still recover the empirical measurement, specifically the induction zone length. Ideally, new chemical mechanisms could be calibrated without imposing vibrational equilibrium, thus rectifying this inconsistency. Until then, we postulate that the non-equilibrium model should accurately reproduce the established empirical measurements, which implicitly account for vibrational non-equilibrium flow physics. As such, we show that $\alpha'_{v,i}$ between 0.4 and 0.6 represents an optimal choice.

As a final note regarding this recommendation for $\alpha'_{v,i}$, we assert that recovering the same steady detonation behaviour between equilibrium and non-equilibrium models does not imply that they will recover the same unsteady detonation behaviour. In particular, it is well established that equilibrium models have trouble accurately predicting detonation cell sizes (Taylor *et al.* 2013*a*; Voelkel *et al.* 2016*a*; Lu *et al.* 2021). However, by introducing non-equilibrium into the model, it is straightforward to show that the signal speed associated with acoustic perturbations changes form (Chu 1957; Clarke 1978). Essentially, the frozen sound speed is now driven by the ratio of specific heats associated with only translational–rotational motion (the equilibrium sound speed still includes the vibrational motion). Depending on the relaxation time scales, and considering that the ratio of specific heats used to define the signal speed is critical for determining the unstable behaviour of the flow (Erpenbeck 1964; Short & Stewart 1998), we expect the non-equilibrium processes to dramatically alter the unsteady behaviour.

5. Features of the chemical–vibrational coupling

We now consider the features associated with our vibrationally informed reaction model. First, we examine the general features of the vibrational efficiency function for typical species in hydrogen combustion, including comparisons with historical models.

5.1. *Vibrational efficiency model features*

With the $\alpha_{v,i}$ defined via (4.9), the general features of the vibrational efficiency function are now examined. The modified vibrational efficiency parameter, $\alpha'_{v,i}$, does not have an established value, except that it is bound between 0 and 1. Thus, we explore its relative effect by examining a range of values. Figure 2 shows the species vibrational efficiency function for common molecules in hydrogen–air combustion with $\alpha'_{v,i}$ varied between 0.3 and 0.7. For each species, we evaluate $Q_{v,i}$ via the harmonic oscillator approximation. As expected, the efficiency function monotonically increases with $T_{v,\mathrm{i}}$ for fixed T_{tr}. Increasing $\alpha'_{v,i}$ pushes the efficiency function farther from unity, amplifying the vibrational non-equilibrium effect, consistent with the reaction diagram shown in figure 1 and our previous discussion (§ 3.3.2). Additionally, molecules with more vibrational degrees of freedom exhibit a greater effect on the vibrational efficiency. This is consistent with the notion that molecules with a greater potential to absorb or expel

https://doi.org/10.1017/jfm.2026.12034 Published online by Cambridge University Press

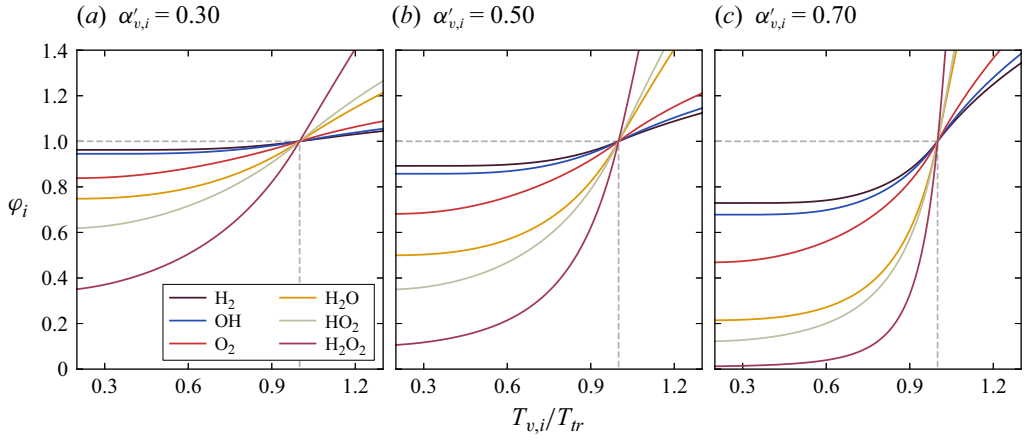


Figure 2. Species vibrational efficiency function versus $T_{v,i}/T_{tr}$ for various molecules in hydrogen combustion, with $T_{tr} = 1500$ K.

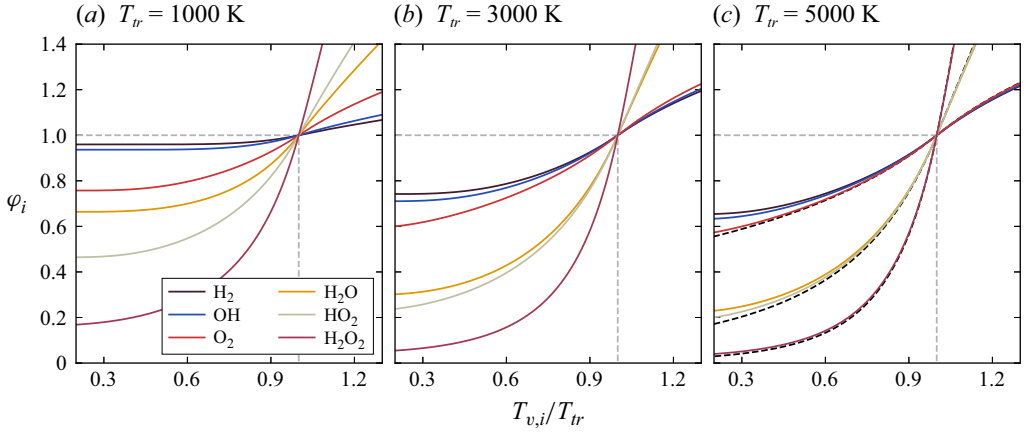


Figure 3. Species vibrational efficiency function versus $T_{v,i}/T_{tr}$ for various molecules in hydrogen combustion, with $\alpha'_{v,i} = 0.5$. The black dashed lines correspond to $[(T_{tr}\Gamma_i)/(T_{v,i}\Gamma_i^{tr})]^{N_{v,i}}$, with $N_{v,i}$ varied between 1, 3 and 6, which corresponds to species with 2, 3 and 4 atoms, respectively.

vibrational energy in molecular collisions will have a greater impact on the reaction rate. For molecules with the same number of vibrational modes, we observe that the vibrational efficiency function scales with the molecule's characteristic vibrational temperatures.

The disparity between molecules with the same number of vibrational modes diminishes as T_{tr} increases, as shown in figure 3, which again shows the species vibrational efficiency function for common molecules in hydrogen–air combustion, now with T_{tr} varied between 1000 and 5000 K. This observation arises from the nature of the vibrational partition function for harmonic oscillators. As T increases, $Q_{v,i}(T)$ becomes proportional to $\prod_{l=1}^{N_{v,i}} T/\theta_{v,il}$, and φ_i becomes proportional to $[(T_{tr}\Gamma_i)/(T_{v,i}\Gamma_i^{tr})]^{N_{v,i}}$. This limit is shown by the black dashed lines in figure 3 at $T_{tr} = 5000$ K, with the various lines corresponding to $N_{v,i} = 1$, 3 and 6, which corresponds to species with 2, 3 and 4 atoms, respectively. By 5000 K, it is clear that the efficiency function has nearly reached its limiting behaviour.

https://doi.org/10.1017/jfm.2026.12034 Published online by Cambridge University Press

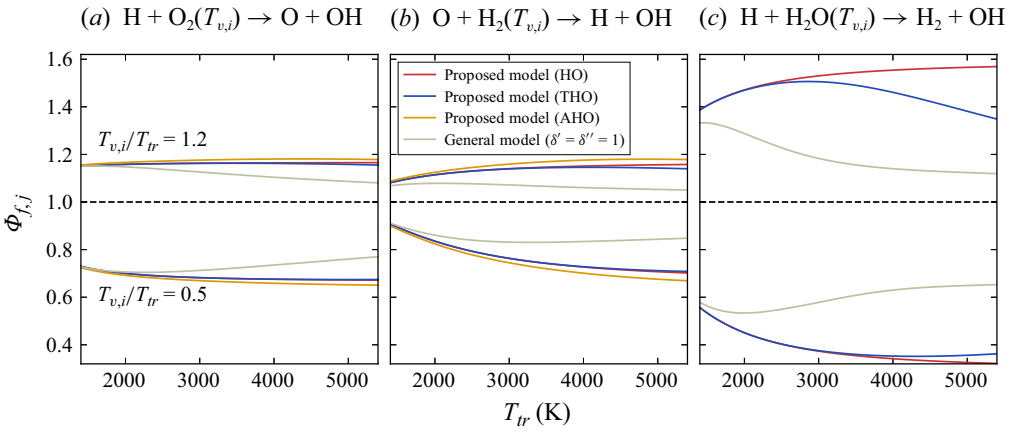


Figure 4. Species vibrational efficiency function versus T_{tr} for various chain-branching reactions in hydrogen combustion, with $\alpha'_{v,i} = 0.5$.

Figure 4 compares how varied partition function definitions affect the efficiency function for chain-branching reactions in hydrogen–air combustion at fixed $T_{v,i}/T_{tr}$ ratios and T_{tr} varied between 1400 and 5400 K. Here, we compare the proposed model, as defined via (4.7), for different energy descriptions: harmonic oscillator (HO), truncated harmonic oscillator (THO) and anharmonic oscillator (AHO). With regard to H_2O, only the HO and THO models are examined. The maximum vibrational energy of each molecule is defined as the dissociation/bond energy of the molecule as collated by Dean (1999).

For vibrationally hot and cold O_2 and H_2, as shown in figures 4(*a*) and 4(*b*), the HO model reproduces similar efficiency function curves to those of the THO and AHO models, suggesting that vibrational energies exceeding the dissociation energy are negligible, and that anharmonic corrections only have a marginal effect. For vibrationally hot and cold H_2O, as shown in figure 4(*c*), the THO and HO models diverge at approximately 3000 K, resulting in a 20 % discrepancy in $\Phi_{f,j}$ at 5000 K, indicating that vibrational energies above the bond energy are non-negligible. This alludes to a significant discrepancy in the limiting behaviour of these two models. As the temperature increases, the partition function associated with the HO model approaches its limit as described for figure 3, whereas the THO model limits to a value proportional to the bond energy. This results in a vibrational efficiency function that limits to one. Thus, at sufficiently high temperatures, the vibrational effect is negligible. A similar limiting behaviour is observed for the AHO model. It is unclear which limiting behaviour is more favourable.

Beyond the HO, THO and AHO models examined in figure 4, we also include the results for the generalised form as defined via (3.19) and (3.20), which limits the vibrational scaling function by the forward and reverse activation energy. Here, we set $\delta' = \delta'' = 1$ and $\beta_f = \beta_r = 0.8$. The general model adopts the AHO description for O_2 and H_2 and the THO model for H_2O. Compared with the proposed model, where $\delta' = \delta'' = 0$, the generalised model reduces the magnitude of the vibrational efficiency function by limiting the impact of the effective vibrational component of the reaction barrier as defined via (3.20). Thus, high-lying vibrational states may be limited by the activation energy, diminishing the vibrational influence on the reaction rate. This is particularly noticeable for larger molecules, as seen with H_2O in figure 4(*c*), which have more vibrational modes and thus a greater vibrational energy.

https://doi.org/10.1017/jfm.2026.12034 Published online by Cambridge University Press

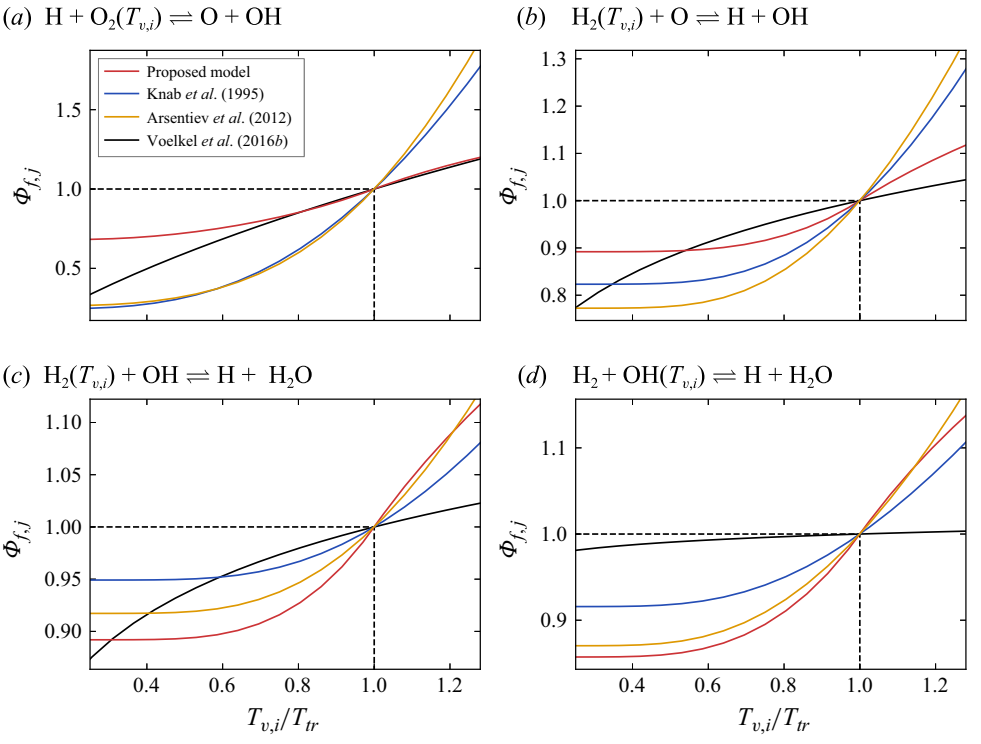


Figure 5. Vibrational efficiency function versus reactant vibrational temperature scaled by T_{tr} for key reactions in hydrogen combustion, with $T_{tr} = 1500\,\mathrm{K}$ and $\alpha_{v,i} = 0.5$.

5.2. *Comparisons with historical models*

Figure 5 shows the vibrational efficiency function for several chain-branching reactions in hydrogen–air detonations, with the proposed model compared with historical models, including the modified Park model presented by Voelkel *et al.* (2016*b*), the CVCV model presented by Knab *et al.* (1995) and the model presented by Arsentiev *et al.* (2012). For the historical models, dissociation and activation energies were taken from Dean (1999) and Burke *et al.* (2012), respectively. For each reaction, we set $T_{tr} = 1500\,\mathrm{K}$ and $\alpha_{v,i} = 0.5$. The modified Park model (Voelkel *et al.* 2016*b*) was directly calibrated to QCT results. Thus, we consider this model to be the target model for these specific reactions. The α parameter associated with the CVCV model was reduced from the recommended value of 0.8 to 0.3 for these comparisons, which provided a much closer match to the modified Park model.

In figure 5(*a*), the vibrational efficiency function of O_2 has a significant effect on the reaction rate. For $T_{v,O_2}/T_{tr} = 0.4$ ($T_{v,O_2} = 600\,\mathrm{K}$), the rate is reduced by approximately 50 % based on the target model. The proposed model closely matches the target model for $T_{v,O_2}/T_{tr} > 0.8$, below which the proposed model begins to flatten out, resulting in less reaction suppression for significantly vibrationally cold states. Both the CVCV and Arsentiev models overestimate the role of vibrational non-equilibrium for both vibrationally hot and cold states, until $T_{v,O_2}/T_{tr} < 0.3$. In figure 5(*b*), vibrational non-equilibrium of H_2 has a lesser effect, with the reaction reduced by 15 % at $T_{v,H_2}/T_{tr} = 0.4$. For vibrational cold flows, each model is within 10 % of the others, with the proposed

https://doi.org/10.1017/jfm.2026.12034 Published online by Cambridge University Press

model exhibiting a slightly lesser vibrational effect. For vibrationally hot flows, the proposed model is significantly closer to the target model.

In figure 5(*c*), the vibrational efficiency function for our proposed model is the same as in figure 5(*b*). However, all of the other models show a reduced vibrational non-equilibrium effect, accounting for the reduced activation energy barrier associated with this reaction. Now, the reaction rate is only reduced by 8 % at $T_{v,\mathrm{H_2}}/T_{tr} = 0.4$. The Knab and Arsentiev models do a better job of capturing this subtle effect, but each model is still within a few percent. In figure 5(*d*), the target model exhibits a marginal non-equilibrium effect, suggesting that OH vibrational non-equilibrium is not relevant for this reaction. None of the other models are able to account for this result, with the Knab model producing the best result.

Two final observations are made regarding figure 5. First, we note that the slope of the efficiency function for the proposed, CVCV and Arsentiev models decreases as $T_{v,i}$ decreases, in contrast to the target model. Subsequently, as $T_{v,i}$ decreases, these models will eventually diverge from the target model. We expect such states to only be observed directly behind the shock (where $T_{v,i}/T_{tr} \approx 0.2$ for a stoichiometric Chapman–Jouguet detonation at standard temperature and pressure). However, we expect the species to relax somewhat quickly to a more moderate vibrationally cold state, where the proposed model is more well suited. Second, the point of this comparison was to validate the choice of our proposed model. We feel that, compared with the significantly more complex historical models (which themselves are not necessarily accurate representations of reality), the proposed model performs well and captures the underlying physics associated with vibrational non-equilibrium's effect on reaction rates.

5.3. *General features of chemical–vibrational exchange*

Chemical–vibrational exchange creates and destroys vibrational energy from chemical reactions and scales with the vibrational energy. Based on the proposed model (4.10), consider (2.10*a*) in non-conservative form, given by

$$\frac{\partial e_{v,i}}{\partial t} + u\frac{\partial e_{v,i}}{\partial x} = \frac{S_{T-V,i} + S_{V-V,i}}{\rho Y_i} + \frac{e_{v,i}(\Gamma_i^{tr}) - e_{v,i}}{\tau_{C-V(c),ij}} - \frac{e_{v,i}(\Gamma_i) - e_{v,i}}{\tau_{C-V(d),ij}}. \tag{5.1}$$

In this form, it is straightforward to show that, for a given species i, positive reactions that create new molecules push $T_{v,i}$ towards Γ_i^{tr} ($e_{v,i} \to e_{v,i}(\Gamma_i^{tr})$). This occurs at a time scale proportional to the species molar production rate scaled by $e_{v,i}(\Gamma_i^{tr})/e_{v,i}^{tr}$. In contrast, negative reactions that destroy molecules push $T_{v,i}$ towards zero ($e_{v,i} \to 0$). This occurs at a time scale proportional to the species molar production rate scaled by $e_{v,i}(\Gamma_i)/e_{v,i}^{tr}$.

Figure 6 shows Γ_i^{tr}/T_{tr} and Γ_i/T_{tr} versus $T_{v,i}/T_{tr}$ for varied values of $\alpha'_{v,i}$. For all vibrational efficiency parameters, $\Gamma_i^{tr}/T_{tr} \geq 1$ as shown in figure 6(*a*), which indicates that vibrational energy is created in a vibrationally hot state. As $T_{v,i}/T_{tr}$ increases beyond 1, this effect becomes diminished. When $\alpha'_{v,i} = 0$ (vibrational energy does not influence reactions), then $\Gamma_i^{tr}/T_{tr} = 1$, so positive reactions push $T_{v,i}$ towards thermal equilibrium, consistent with (5.1).

Figure 6(*b*) shows how the destruction of vibrational energy scales with Γ_i and $T_{v,i}$. When the species is vibrationally hot ($T_{v,i}/T_{tr} > 1$), then $\Gamma_i/T_{tr} \gg 1$ and $e_{v,i}(\Gamma_i)/e_{v,i}^{tr} \gg 1$, leading to rapid depletion of vibrational energy. As the species becomes vibrationally cold, then the destruction rate of vibrational energy goes to zero. When $\alpha'_{v,i} = 0$, then $\Gamma_i = T_{v,i}$ and, similarly, the destruction rate goes to zero as shown in (5.1). Thus, negative reactions do not alter the local vibrational energy.

https://doi.org/10.1017/jfm.2026.12034 Published online by Cambridge University Press

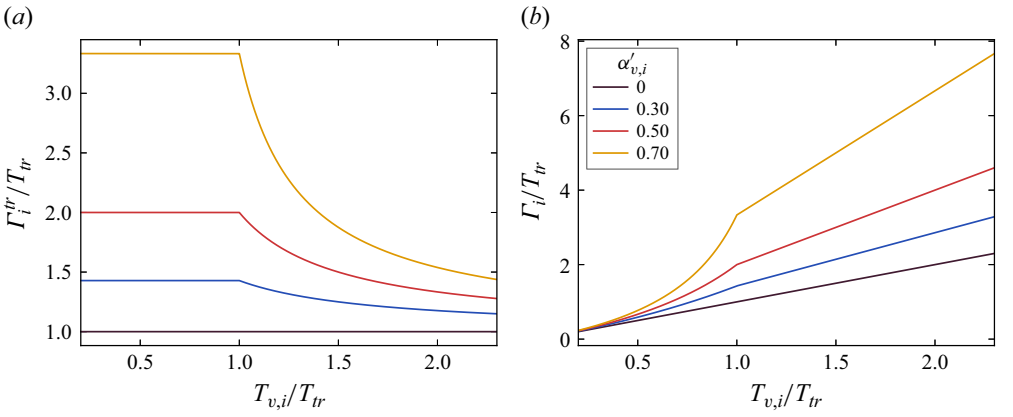


Figure 6. Gamma temperatures versus vibrational temperature, both relative to T_{tr}.

6. Conclusions

In this work, we have presented a robust framework for modelling high-speed flows with vibrational non-equilibrium, including supersonic combustion and detonations. Continuum-scale governing equations for a vibrational non-equilibrium flow were employed with a vibrationally partitioned equation of state and partial pressure mixing model. We then developed a general set of constitutive relations for vibrational non-equilibrium, including T–V exchange to model relaxation and V–V exchange to model redistribution. In particular, for V–V exchange, a new form for the V–V exchange probability was employed to ensure consistency at thermal equilibrium and to prevent leakage from vibrational modes into translational energy.

Vibrationally informed chemical reactions were modelled via a generalised vibrational efficiency function for detailed kinetics that is consistent with the principle of detailed balance. This model represents an extension and generalisation of historical models, now derived for an arbitrary set of reactants and products with additional consideration for reverse reactions. From this kinetic scheme, consistent C–V exchange rates were derived to control the formation and destruction of vibrational energy from chemical reactions, resulting in a CVCV model.

This modelling framework was applied to high-speed combustion applications, with a specific focus on reactive flows at temperatures below 5000 K. First, we assume that the vibrational energy of each species can be modelled via the harmonic oscillator approximation, which is valid when high-lying vibrational modes near the dissociation energy are marginally populated and anharmonic effects are negligible. For T–V exchange, we recommend using the time scale presented by Millikan & White (1963), noting that high-temperature corrections have a negligible impact on the relaxation time scale below 10 000 K. With regard to V–V exchange, we recommend setting the V–V exchange probability, $P'_{V-V,ij}$, to a constant value, consistent with historical studies. However, based on our analysis in Part 2 (Voelkel *et al.* 2026) examining steady relaxation profiles of hydrogen–air mixtures, this value should be decreased considerably compared with the historical value used in high-temperature regimes, specifically from 10^{-2} to 10^{-4}. For vibrationally informed chemical reactions, we neglect the activation energy component of the vibrational scaling function, resulting in a simplified vibrational efficiency function dependent on the vibrational partition function of each species. The C–V exchange rate is simplified accordingly. The final model utilises a species-specific vibrational efficiency parameter, $\alpha'_{v,i}$, defined between zero and one, to control the relative effect of vibrational

https://doi.org/10.1017/jfm.2026.12034 Published online by Cambridge University Press

non-equilibrium on chemical reactions. Based on our analysis in Part 2 (Voelkel *et al.* 2026) examining steady detonation profiles of hydrogen–air mixtures, we recommend setting $\alpha'_{v,i}$ between 0.4 and 0.6.

The reduced efficiency function was examined in the context of its general features, limiting behaviour and accuracy compared with historical models. The model was found to produce favourable physical effects and compared well with the historical models. Overall, the proposed model rigorously considers vibrational non-equilibrium processes within the high-speed combustion regime in an inclusive and consistent modelling framework. The result is a tractable, physically consistent and robust model for examining arbitrary reactive systems in the high-speed combustion regime.

Declaration of interests. The authors report no conflict of interest.

Appendix A. Rotational non-equilibrium and free-electron motion

The model presented in this work is focused on capturing vibrational non-equilibrium effects. However, it is relatively straightforward to extend this model to account for other non-equilibrium effects. To account for rotational non-equilibrium and free-electron motion, we still assume that some subset of the internal energy components can be described by a 'common' or bulk translational temperature, denoted T_t. Energy components not described by T_t can experience mode-specific non-equilibrium. The sets of species that experience translational, rotational, vibrational and electronic non-equilibrium are denoted Ω_α, with $\alpha = t, r, v$ or el, depending on the mode. We define the common components of the internal energy from (2.5) as

$$e_c(T_t) = \sum_{i \notin \Omega_t} Y_i e_{t,i}(T_t) + \sum_{i \notin \Omega_r} Y_i e_{r,i}(T_t) + \sum_{i \notin \Omega_v} Y_i e_{v,i}(T_t) + \sum_{i \notin \Omega_{el}} Y_i e_{el,i}(T_t). \tag{A1}$$

To reduce the complexity, we assume that Ω_{el} is empty (the electronic component of the energy is always in equilibrium) and that Ω_t only contains free electrons. The resulting mixture's internal energy and pressure are given by

$$e = e_c(T_t) + Y_e e_{t,e} + \sum_{i \in \Omega_r} Y_i e_{r,i} + \sum_{i \in \Omega_v} Y_i e_{v,i}, \quad p = \rho R T_t + \rho Y_e R_e (T_e - T_t), \tag{A2}$$

where the e subscript denotes the free-electron species and T_e is the electron (translational) temperature. Following the procedure in § 2.2, we arrive at a series of transport equations for the rotational, vibrational and free-electron energy components:

$$\frac{\partial}{\partial t}\left(\rho Y_i e_{r,i}\right) + \frac{\partial}{\partial x}\left(\rho u Y_i e_{r,i}\right) = S_{R-T,i} + S_{R-R,i} + S_{R-V,i} + S_{R-E,i} + S_{R-C,i}, \; i \in \Omega_r, \tag{A3a}$$

$$\frac{\partial}{\partial t}\left(\rho Y_i e_{v,i}\right) + \frac{\partial}{\partial x}\left(\rho u Y_i e_{v,i}\right) = S_{V-T,i} + S_{V-R,i} + S_{V-V,i} + S_{V-E,i} + S_{V-C,i}, \; i \in \Omega_v, \tag{A3b}$$

$$\frac{\partial}{\partial t}\left(\rho Y_e e_e\right) + \frac{\partial}{\partial x}\left(\rho u Y_e e_e\right) = S_{E-T,i} + S_{E-R,i} + S_{E-V,i} + S_{E-C,i}, \tag{A3c}$$

where $S_{R-T,i}$, $S_{R-R,i}$, etc., denote the set of exchange terms between each energy mode. Defining each of the exchange terms is beyond the scope of this study, but as a first approximation, assuming that rotational relaxation is rapid, one might neglect rotational–rotational, vibrational–rotational, electron–rotational and chemical–rotational exchange

https://doi.org/10.1017/jfm.2026.12034 Published online by Cambridge University Press

effects. Then,

$$\frac{\partial}{\partial t}\left(\rho Y_i e_{r,i}\right) + \frac{\partial}{\partial x}\left(\rho u Y_i e_{r,i}\right) = \frac{\rho Y_i (e^t_{r,i} - e_{r,i})}{\tau_{R-T,i}} + \dot{\omega}_i e_{r,i}, \tag{A4}$$

for $i \in \Omega_r$, where $e^t_{r,i}$ denotes the rotational energy evaluated at T, and $\tau_{R-T,i}$ is the rotational–translational relaxation time scale (see Boyd (1990*a*) and Panesi *et al.* (2013) for more details). The reaction term ensures that chemical reactions do not modify the rotational energy. Likewise, it is common to assume that electron–vibrational energy coupling is weak, so

$$\frac{\partial}{\partial t}\left(\rho Y_i e_e\right) + \frac{\partial}{\partial x}\left(\rho u Y_i e_e\right) = \frac{\rho Y_i (e^t_e - e_e)}{\tau_{E-T,i}} + \dot{\omega}_e e_e, \tag{A5}$$

where e^t_{e} denotes the electron energy evaluated at T, and $\tau_{E-T,i}$ is the electron–translational relaxation time scale (see Lee (1985) and Candler & MacCormack (1988, 1991) for more details). The exchange terms for the vibrational energy are consistent with those defined in § 3, assuming vibrational–rotational and vibrational–electron exchange terms are negligible. Thus, preliminary studies that account for rotational non-equilibrium and free-electron motion only need to define $\tau_{R-T,i}$ and $\tau_{E-T,i}$. Of course, (A4) and (A5) are only meant to provide a starting point, and one would then build upon these models to include other coupled exchange effects where appropriate. For instance, Candler & MacCormack (1988, 1991) note that the vibrational–electron exchange process is relatively weak for most species, but N_2 exhibits a strong coupling effect. Depending on the flow regime, the resulting model might need to account for this and other similarly relevant processes.

References

Adamovich, I.V., Macheret, S.O., Rich, J.W. & Treanor, C.E. 1995 Vibrational relaxation and dissociation behind shock waves. Part 1 – Kinetic rate models. *AIAA J.* **33** (6), 1064–1069.

Arsentiev, I., Loukhovitski, B. & Starik, A. 2012 Application of state-to-state approach in estimation of thermally nonequilibrium reaction rate constants in mode approximation. *Chem. Phys.* **398**, 73–80.

Atkins, P.W., De Paula, J. & Keeler, J. 2023 *Atkins' Physical Chemistry*. Oxford University Press.

Boyd, I.D. 1990*a* Rotational–translational energy transfer in rarefied nonequilibrium flows. *Phys. Fluids A* **2** (3), 447–452.

Boyd, I.D. 1990*b* Rotational and vibrational nonequilibrium effects in rarefied hypersonic flow. *J. Thermophys. Heat Transfer* **4** (4), 478–484.

Boyd, I.D. & Schwartzentruber, T.E. 2017 *Nonequilibrium Gas Dynamics and Molecular Simulation*. Cambridge University Press.

Burke, M.P., Chaos, M., Ju, Y., Dryer, F.L. & Klippenstein, S.J. 2012 Comprehensive H_2/O_2 kinetic model for high-pressure combustion. *Intl J. Chem. Kinet.* **44** (7), 444–474.

Candler, G.V. 2019 Rate effects in hypersonic flows. *Annu. Rev. Fluid Mech.* **51** (1), 379–402.

Candler, G.V. & MacCormack, R.W. 1988 The computation of hypersonic ionized flows in chemical and thermal nonequlibrium. In *26th Aerospace Sciences Meeting*, p. 511. AIAA.

Candler, G.V. & MacCormack, R.W. 1991 Computation of weakly ionized hypersonic flows in thermochemical nonequilibrium. *J. Thermophys. Heat Transfer* **5** (3), 266–273.

Center, R. & Newton, J. 1978 Vibrational relaxation of N_2 by H_2O. *J. Chem. Phys.* **68** (8), 3327–3333.

Chaudhry, R.S. & Candler, G.V. 2019 Statistical analyses of quasiclassical trajectory data for air dissociation. In *AIAA Scitech 2019 Forum*, p. 0789. AIAA.

Chaudhry, R.S., Torres, E., Schwartzentruber, T.E. & Candler, G.V. 2025 Modified Marrone–Treanor dissociation model: formulation and benchmarking for diatom/atom mixtures. arXiv: 2506.06236.

Chavez, S.B.R., Chatelain, K.P. & Lacoste, D.A. 2023 Two-dimensional visualization of induction zone in hydrogen detonations. *Combust. Flame* **255**, 112905.

Chu, B.T. 1957 *Wave Propagation and the Method of Characteristics in Reacting Gas Mixtures with Applications to Hypersonic Flow*, Technical report (Brown University. Division of Engineering). Wright Air Development Center, Air Research Development and Command, United States Air Force.

https://doi.org/10.1017/jfm.2026.12034 Published online by Cambridge University Press

CLARKE, J. 1978 Gas dynamics with relaxation effects. *Rep. Prog. Phys.* **41** (6), 807.
DEAN, J.A. 1999 *Lange's Handbook of Chemistry*. McGraw-Hill: Inc.
DU, Y., SUN, S., TAN, M., HUANG, H., YAN, C., MENG, X., CHEN, X. & WANG, H. 2023 Numerical study on the non-equilibrium characteristics of high-speed atmospheric re-entry flow and radiation of aircraft based on fully coupled model. *J. Fluid Mech.* **977**, A39.
ERPENBECK, J.J. 1964 Stability of idealized one-reaction detonations. *Phys. Fluids* **7** (5), 684–696.
ESPOSITO, F., ARMENISE, I. & CAPITELLI, M. 2006 N–N_2 state to state vibrational-relaxation and dissociation rates based on quasiclassical calculations. *Chem. Phys.* **331** (1), 1–8.
FIÉVET, R. & RAMAN, V. 2018 Effect of vibrational nonequilibrium on isolator shock structure. *J. Propul. Power* **34** (5), 1334–1344.
FIÉVET, R., VOELKEL, S., KOO, H., RAMAN, V. & VARGHESE, P.L. 2017 Effect of thermal nonequilibrium on ignition in scramjet combustors. *Proc. Combust. Inst.* **36** (2), 2901–2910.
FISHER, E.R. & KUMMLER, R.H. 1968 Relaxation by vibration–vibration exchange processes. Part II. Binary mixtures. *J. Chem. Phys.* **49** (3), 1085–1093.
FURUDATE, M., FUJITA, K. & ABE, T. 2006 Coupled rotational-vibrational relaxation of molecular hydrogen at high temperatures. *J. Thermophys. Heat Transfer* **20** (3), 457–464.
GALLIS, M.A., BOND, R.B. & TORCZYNSKI, J.R. 2010 Assessment of collisional-energy-based models for atmospheric species reactions in hypersonic flows. *J. Thermophys. Heat Transfer* **24** (2), 241–253.
GNOFFO, P.A. 1999 Planetary-entry gas dynamics. *Annu. Rev. Fluid Mech.* **31** (1), 459–494.
HALL, J.G., ESCHENROEDER, A.Q. & MARRONE, P.V. 1962 Blunt-nose inviscid airflows with coupled nonequilibrium processes. *J. Aerosp. Sci.* **29** (9), 1038–1051.
HAMMERLING, P., TEARE, J. & KIVEL, B. 1959 Theory of radiation from luminous shock waves in nitrogen. *Phys. Fluids* **2** (4), 422–426.
KADOCHNIKOV, I. & ARSENTIEV, I. 2020 Modelling of vibrational nonequilibrium effects on the H_2–air mixture ignition under shock wave conditions in the state-to-state and mode approximations. *Shock Waves* **30** (5), 491–504.
KEE, R.J., RUPLEY, F.M. & MILLER, J.A. 1989 Chemkin-II: a Fortran chemical kinetics package for the analysis of gas-phase chemical kinetics. *Tech. Rep.* SAND-89-8009. Sandia National Laboratory, Livermore, CA, USA.
KNAB, O., FRÜHAUF, H.H. & JONAS, S. 1992 Multiple temperature descriptions of reaction rate constants with regard to consistent chemical-vibrational coupling. In *27th Thermophysics Conference*, p. 2947. AIAA.
KNAB, O., FRÜHAUF, H.H. & MESSERSCHMID, E. 1995 Theory and validation of the physically consistent coupled vibration-chemistry-vibration model. *J. Thermophys. Heat Transfer* **9** (2), 219–226.
KOO, H., RAMAN, V. & VARGHESE, P.L. 2015 Direct numerical simulation of supersonic combustion with thermal nonequilibrium. *Proc. Combust. Inst.* **35** (2), 2145–2153.
KUNG, R. & CENTER, R. 1975 High temperature vibrational relaxation of H_2O by H_2O, He, Ar, and N_2. *J. Chem. Phys.* **62** (6), 2187–2194.
LANDAU, L. & TELLER, E. 1936 On the theory of sound dispersion. *Phys. Z. Sowjetunion* **10**, 34–38.
LEE, J.H. 1985 Electron-impact vibrational excitation rates in the flow field of aeroassisted orbital transfer vehicles. In *20th Thermophysics Conference*, p. 1035. AIAA.
LEE, R.S. 1965 Hypersonic non-equilibrium flow over slender bodies. *J. Fluid Mech.* **22** (3), 417–431.
LEMMON, E.W., BELL, I.H., HUBER, M.L. & MCLINDEN, M.O. 2024 Thermophysical properties of fluid systems. In *NIST Chemistry WebBook 69*, NIST Standard Reference Database Number 69 (ed. P.J. Linstrom & W.G. Mallard). National Institute of Standards and Technology.
LU, X., KAPLAN, C.R. & ORAN, E.S. 2021 A chemical-diffusive model for simulating detonative combustion with constrained detonation cell sizes. *Combust. Flame* **230**, 111417.
LUKHOVITSKII, B., STARIK, A. & TITOVA, N. 2008 Thermally nonequilibrium processes occurring during the ignition of hydrocarbon-air mixtures behind shock waves. *Russian J. Phys. Chem. B* **2** (5), 722–731.
MACHERET, S.O. & ADAMOVICH, I.V. 2000 Semiclassical modeling of state-specific dissociation rates in diatomic gases. *J. Chem. Phys.* **113** (17), 7351–7361.
MARRONE, P.V. & TREANOR, C.E. 1963 Chemical relaxation with preferential dissociation from excited vibrational levels. *Phys. Fluids* **6** (9), 1215–1221.
MCQUARRIE, D.A. 2000 *Statistical Mechanics*. University Science Books.
MILLIKAN, R.C. & WHITE, D.R. 1963 Systematics of vibrational relaxation. *J. Chem. Phys.* **39** (12), 3209–3213.
MUNAFÒ, A., LIU, Y. & PANESI, M. 2015 Modeling of dissociation and energy transfer in shock-heated nitrogen flows. *Phys. Fluids* **27** (12), 127101.
PANESI, M., JAFFE, R.L., SCHWENKE, D.W. & MAGIN, T.E. 2013 Rovibrational internal energy transfer and dissociation of $N_2(^1\Sigma_g^+) - N(^4S_u)$ system in hypersonic flows. *J. Chem. Phys.* **138** (4), 044312.

https://doi.org/10.1017/jfm.2026.12034 Published online by Cambridge University Press

PANESI, M., MUNAFÒ, A., MAGIN, T. & JAFFE, R. 2014 Nonequilibrium shock-heated nitrogen flows using a rovibrational state-to-state method. *Phys. Rev. E* **90** (1), 013009.

PARK, C. 1988 Assessment of a two-temperature kinetic model for dissociating and weakly ionizing nitrogen. *J. Thermophys. Heat Transfer* **2** (1), 8–16.

PARK, C. 1989 Assessment of two-temperature kinetic model for ionizing air. *J. Thermophys. Heat Transfer* **3** (3), 233–244.

PARK, C. 1993 Review of chemical-kinetic problems of future NASA missions, I: earth entries. *J. Thermophys. Heat Transfer* **7** (3), 385–398.

PASSIATORE, D., SCIACOVELLI, L., CINNELLA, P. & PASCAZIO, G. 2022 Thermochemical non-equilibrium effects in turbulent hypersonic boundary layers. *J. Fluid Mech.* **941**, A21.

POWERS, J.M. & PAOLUCCI, S. 2005 Accurate spatial resolution estimates for reactive supersonic flow with detailed chemistry. *AIAA J.* **43** (5), 1088–1099.

REISING, H.H., HALLER, T.W., CLEMENS, N.T., VARGHESE, P.L., FIÉVET, R. & RAMAN, V. 2016 Spontaneous Raman scattering temperature measurements and large eddy simulations of vibrational non-equilibrium in high-speed jet flames. In *32nd AIAA Aerodynamic Measurement Technology and Ground Testing Conference*, p. 3550. AIAA.

SCHRAMM, J.M., HANNEMANN, K. & HORNUNG, H.G. 2023 Hypersonic flow over spherically blunted cone capsules for atmospheric entry. Part 2. Vibrational non-equilibrium effects. *J. Fluid Mech.* **954**, A32.

SCHWARTZ, R., SLAWSKY, Z. & HERZFELD, K. 1952 Calculation of vibrational relaxation times in gases. *J. Chem. Phys.* **20** (10), 1591–1599.

SECREST, D. 1973 Theory of rotational and vibrational energy transfer in molecules. *Annu. Rev. Phys. Chem.* **24** (1), 379–406.

SHI, L., SHEN, H., ZHANG, P., ZHANG, D. & WEN, C. 2017 Assessment of vibrational non-equilibrium effect on detonation cell size. *Combust. Sci. Technol.* **189** (5), 841–853.

SHI, X., JAYARAMAN, A.S. & WANG, H. 2024 Probing vibrational nonequilibrium in detonations with ozone. *Proc. Combust. Inst.* **40** (1–4), 105695.

SHORT, M. & STEWART, D.S. 1998 Cellular detonation stability. Part 1. A normal-mode linear analysis. *J. Fluid Mech.* **368**, 229–262.

STARIK, A. & TITOVA, N. 2001 Kinetic mechanisms for the initiation of supersonic combustion of a hydrogen-air mixture behind a shock wave under the excitation of molecular vibrations in initial reagents. *Tech. Phys.* **46**, 929–940.

TAYLOR, B., KESSLER, D., GAMEZO, V. & ORAN, E. 2013*a* Numerical simulations of hydrogen detonations with detailed chemical kinetics. *Proc. Combust. Inst.* **34** (2), 2009–2016.

TAYLOR, B.D., KESSLER, D.A. & ORAN, E.S. 2013*b* Estimates of vibrational nonequilibrium time scales in hydrogen-air detonation waves. In *24th International Colloquium on the Dynamics of Explosive and Reactive Systems*. Institute for Dynamics of Explosions and Reactive Systems (IDERS).

TAYLOR, R., CAMAC, M. & FEINBERG, R. 1967 Measurements of vibration-vibration coupling in gas mixtures. *Symp. (Intl) Combust.* **11** (1), 49–65.

TREANOR, C.E. & MARRONE, P.V. 1962 Effect of dissociation on the rate of vibrational relaxation. *Phys. Fluids* **5** (9), 1022–1026.

UY, K.C., SHI, L. & WEN, C. 2018 Chemical reaction mechanism related vibrational nonequilibrium effect on the Zel'dovich–von Neumann–Döring (ZND) detonation model. *Combust. Flame* **196**, 174–181.

VARGA, Z., MEANA-PAÑEDA, R., SONG, G., PAUKKU, Y. & TRUHLAR, D.G. 2016 Potential energy surface of triplet N_2O_2. *J. Chem. Phys.* **144** (2), 024310.

VARGAS, J., MÉVEL, R., LINO DA SILVA, M. & LACOSTE, D. 2022 Development of a steady detonation reactor with state-to-state thermochemical modeling. *Shock Waves* **32** (8), 679–689.

VARMA, A.R. & ZHONG, X. 2025 Hypersonic boundary-layer receptivity to free-stream acoustic waves with thermochemical non-equilibrium effects. *J. Fluid Mech.* **1013**, A16.

VINCENTI, W.G. & KRUGER, C.H. 1965 *Introduction to Physical Gas Dynamics*, 2nd edn. Krieger Publishing Company.

VOELKEL, S., MASSELOT, D., VARGHESE, P.L. & RAMAN, V. 2016*a* Analysis of hydrogen-air detonation waves with vibrational nonequilibrium. *AIP Conf. Proc.* **1786** (1), 070015.

VOELKEL, S., RAMAN, V. & VARGHESE, P.L. 2016*b* Effect of thermal nonequilibrium on reactions in hydrogen combustion. *Shock Waves* **26** (5), 539–549.

VOELKEL, S.J. 2016 Thermal nonequilibrium models for high-temperature reactive processes. PhD thesis, The University of Texas at Austin.

VOELKEL, S.J., SHORT, M. & CHIQUETE, C. 2026 Vibrational nonequilibrium in high-speed combustion applications. 2. Steady flow analysis. *J. Fluid Mech.* (submitted).

https://doi.org/10.1017/jfm.2026.12034 Published online by Cambridge University Press

WHITE, D. 1968 Shock-tube study of vibrational exchange in N_2–O_2 mixtures. *J. Chem. Phys.* **49** (12), 5472–5476.

WRAY, K.L. & TEARE, J.D. 1962 Shock-tube study of the kinetics of nitric oxide at high temperatures. *J. Chem. Phys.* **36** (10), 2582–2596.

YANG, C., HUANG, H. & SUN, Q. 2019 A microscopic study of one-dimensional H_2-O_2 detonation using DSMC method. *AIP Conf. Proc.* **2132** (1), 070013.

ZANARDI, I., VENTURI, S. & PANESI, M. 2023 Adaptive physics-informed neural operator for coarse-grained non-equilibrium flows. *Sci. Rep.* **13** (1), 15497.

ZANGENE, F. & RADULESCU, M.I. 2025 Role of the argon and helium bath gases on the structure of H_2/O_2 detonations. *Combust. Flame* **280**, 114381.

https://doi.org/10.1017/jfm.2026.12034 Published online by Cambridge University Press